Olivine major and trace element compositions coupled with spinel chemistry to unravel the magmatic systems feeding monogenetic basaltic volcanoes

M. Éva Jankovics[1a, *]

m.eva.jankovics@gmail.com

Tamás Sági[1a, 2b]

Rebecca L. Astbury[3c]

Maurizio Petrelli[3c]

Balázs Kiss[1a, 4d]

Teresa Ubide[5e]

Károly Németh[6f]

Theodoros Ntaflos[7g]

Szabolcs Harangi[1a, 2b]

[1a]MTA-ELTE Volcanology Research Group, Pázmány Péter sétány 1/C, 1117 Budapest, Hungary

[2b]Department of Petrology and Geochemistry, Eötvös Loránd University, Pázmány Péter sétány 1/C, 1117 Budapest, Hungary

[3c]Petro-Volcanology Research Group, Department of Physics and Geology, Università degli Studi di Perugia, Piazza dell'Università 1, 06123 Perugia, Italy

[4d]Institute of Geography and Earth Sciences, Eötvös Loránd University, Pázmány Péter sétány 1/C, 1117 Budapest, Hungary

[5e]School of Earth and Environmental Sciences, The University of Queensland, Brisbane, QLD 4072, Australia

[6f]Institute of Agriculture and Environment, Massey University, Private Bag 11222, Palmerston North, New Zealand

[7g]Department of Lithospheric Research, University of Vienna, Althanstrasse 14, 1090 Vienna, Austria

*Corresponding author.

Abstract

Monogenetic basaltic volcanic systems, despite their considerable smaller size and shorter lifetime compared to polygenetic volcanoes, can have complex pre-eruptive histories and composite volcanic facies architectures. Their source-to-surface investigation is essential for our better understanding of monogenetic volcanism and requires high-resolution mineral-scale analyses.

In this study, we focus on diversely zoned olivine crystals and their spinel inclusions from alkaline basaltic volcanics that are the result of mixing of numerous magmas, crystals and fragments of various origins. The Fekete-hegy volcanic complex is one of the largest and most composite eruptive centers in the intracontinental monogenetic Bakony–Balaton Highland Volcanic Field (western Pannonian Basin, Eastern Central Europe). It is a compound multi-vent system built up by multiple eruption episodes: initial maar-forming phreatomagmatic eruptions were followed by massive lava flows and magmatic explosive activity. We performed stratigraphically controlled sampling in order to reveal the history of the successively erupted magma batches represented by the distinct eruptive units, as well as to discover the petrogenetic processes that controlled the evolution of the magmatic system.

The juvenile pyroclasts of the phreatomagmatic eruption products (unit 1) contain a remarkably diverse mineral assemblage including five different olivine types and three distinct spinel groups. In addition, they comprise various xenoliths. Based on detailed textural investigations combined with in situ electron microprobe analyses, high-resolution laser ablation ICP-MS trace element mapping and single spot measurements on the

variably zoned olivines of unit 1 samples, eight distinct environments are inferred to have been involved in their formation. Four of these environments account for the significant compositional variation of the olivine-hosted spinel inclusions. A complex set of open- and closed-system petrogenetic processes operated during the evolution of the magmatic system: magma stalling, accumulation, storage, fractionation, mixing, replenishments, cumulate remobilization, incorporation of foreign fragments and crystals from the wall rocks. All these diverse environments and processes resulted in the mixed character of the erupted magmas during the initial phreatomagmatic eruptive phase.

In contrast, the uniform petrological features and the small variations shown by the olivines and spinels from unit 2-3 indicate that the later magmatic explosive – effusive phase was preceded by a considerable change in the magmatic system; it experienced a simple evolution through olivine + spinel fractional crystallization without any of the complexities seen during the initial phase.

The present study emphasizes the importance of high-resolution mineral-scale textural and chemical investigations to unravel the complexity of the sub-volcanic magmatic systems feeding monogenetic basaltic volcanoes. Compared to the application of whole-rock geochemistry alone, this approach enables a direct and more detailed insight into the architecture and evolution of these systems.

Keywords: Crystal growth stratigraphy; LA-ICP-MS; Monogenetic volcanism; Olivine; Open-system processes; Spinel

1.1 Introduction

Mineral-scale studies on various volcanic rocks have long been demonstrated as being key to understanding sub-volcanic systems. As minerals respond both texturally and compositionally to changing magmatic environments, they retain abundant information concerning the history of magmatic compositions and processes in their crystal growth stratigraphy (e.g., Davidson et al., 2007; Ginibre et al., 2007; Blundy and Cashman, 2008; Streck, 2008). Thus, detailed investigation of the textures, zoning patterns and compositions of rock-forming minerals allows us to detect distinct populations and to reveal the origins of single crystals, making it a powerful tool in discovering the evolution of magmatic systems.

Olivine crystals are valuable recorders of deep-seated petrogenetic processes and involved magmas. Their high-resolution textural, zoning and chemical analysis provides a particular insight into the pre-eruptive evolution of various magmatic systems (e.g., Landi et al., 2009; Kahl et al., 2011, 2013, 2015, 2017; Martí et al., 2013; Ruprecht and Plank, 2013; Longpré et al., 2014; ~~Bouvet~~ de Maisonneuve et al., 2016; Oeser et al., 2018). Additionally, spinel that crystallizes as one of the liquidus phases in primitive mantle-derived magmas has proven to be a useful petrogenetic indicator, sensitively reflecting the melt composition (e.g., Irvine, 1965, 1967; Dick and Bullen, 1984; Allan et al., 1988; Arai, 1992; Roeder, 1994; Clynne and Borg, 1997; Kamenetsky et al., 2001; Roeder et al., 2003). Integrating all the information yielded by these two early crystallizing phases in mafic magmas enables us to untangle in detail the processes of partial melting and crystallization of basaltic magmas, as well as to unveil complexities during their ascent histories (e.g., Reubi et al., 2002; Smith and Leeman, 2005; Jankovics et al., 2012, 2015; Harangi et al., 2013). Contrary to the direct and comprehensive insight these minerals provide, whole-rock geochemistry usually obscures the real details of magmatic evolution since it represents the resultant (erupted magma) composition, often derived from a complex set of distinct magma pockets having interacted through various processes and recycled an assortment of crystals (e.g., Reubi and Blundy, 2009; Ubide et al., 2014).

In spite of this, detailed studies on monogenetic basaltic volcanic centers – which have already been proven to be formed by complex volcanological and pre-eruptive histories – generally only rest on whole-rock major, trace element and isotopic compositions that show significant compositional variations through their successions and between eruptive phases. These variations are attributed to complex melting and mixing processes within the mantle sources, changes in melting conditions and mixing of different magma batches during ascent (e.g., Strong and Wolff, 2003; Smith et al., 2008; Brenna et al., 2010, 2011; Erlund et al., 2010; McGee et al., 2012; Sohn et al., 2012; van Otterloo et al., 2014; Boyce et al., 2015). Conversely, in-depth mineral-scale investigations on basaltic volcanics from distinct eruptive units through the sequence of an individual monogenetic complex (or center) have only scarcely been performed (e.g., Jankovics et al., 2015; Gernon et al., 2016; Re et al., 2017).

In recent decades, extensive investigations on monogenetic volcanic fields suggest that different (simple vs. complex) petrographic types of small-volume basalts can be distinguished. Numerous examples are known for petrographically simple monogenetic products which are common in all volcanic fields (e.g., McGee and Smith, 2016; Brenna et al., 2018) hosting only a simple phenocryst assemblage (olivine ± clinopyroxene) potentially accompanied by xenoliths + xenocrysts. In contrast, petrographically complex basaltic rocks – comprising diverse crystal populations with variable zoning and disequilibrium features – from monogenetic ~~centres~~ centers have been reported more rarely (e.g., Jankovics et al., 2013, 2015; Re et al., 2017).

This paper focuses on the Fekete-hegy volcanic complex which is one of the largest (~12 km^2) and most composite eruptive centers in the intracontinental monogenetic Bakony–Balaton Highland Volcanic Field (western Pannonian Basin, Eastern Central Europe). It is characterized by a complex volcanic facies architecture consisting of the phreatomagmatic products of at least four maars overlain by massive lava flows and two scoria cones (e.g., Auer et al., 2007), suggesting multiple eruption episodes. In this study, we carried out stratigraphically controlled sampling in order to characterize the successively erupted magma batches represented by the distinct eruptive units, as well as to reveal the petrogenetic processes that occurred during their ascent histories.

Here, we investigate complex populations of olivine crystals and their spinel inclusions in the alkaline basaltic volcanics of the Fekete-hegy volcanic complex, which serve as an excellent example for basaltic rocks resulting from the interaction of numerous melts, crystals and fragments of various origins. Detailed textural investigations (with SEM) and in situ EMPA analyses were combined with LA-ICP-MS trace element mapping and single spot measurements to unravel the remarkably diverse olivine zoning record. High-resolution LA-ICP-MS trace element mapping of igneous minerals (clinopyroxenes, amphiboles, feldspars, olivines) has been used to unveil the complex evolution of magma plumbing systems by only a few studies so far (Ubide et al., 2015; Kahl et al., 2017; Astbury et al., 2018; Ubide and Kamber, 2018), which infer this technique is a promising and useful tool. The present study is the first example of the application of this method to detect olivine compositional zoning at the trace element level in monogenetic basaltic systems. Our aim is to explore the olivine and spinel assemblage to discover the pre-eruptive evolution of the magmatic system beneath the Fekete-hegy volcanic complex through its entire lifespan.

2.2 Geological setting

The Carpathian–Pannonian Region is situated in the north-eastern part of the Alpine–Mediterranean region and comprises the Carpathians arcuate orogenic belt and the Pannonian Basin behind it (Fig. 1A). The Pannonian Basin is a Miocene extensional back-arc basin surrounded by the Alpine, Carpathian and Dinarides orogenic belts. It is characterized by thin lithosphere (50–80 km) and crust (22–30 km) coupled with high heat flow (up to 140 mW/m^2; e.g., Csontos et al., 1992; Fodor et al., 1999; Tari et al., 1999; Bada and Horváth, 2001; Lenkey et al., 2002; Horváth et al., 2006, 2015). These characteristics are the results of the initial *syn*-rift phase (ca. 20–12 Ma; Horváth et al., 2006) of the Pannonian Basin that involved back-arc extension and significant thinning of the lithosphere. Various hypotheses exist for the driving mechanism of the considerable lithospheric extension (e.g., gravitational collapse of the over-thickened lithosphere, subduction roll-back, asthenospheric flow from the Alpine collision zone) that are summarized by Harangi et al. (2015) (and references therein). The Late Miocene–Pliocene post-rift phase was accompanied by thermal subsidence, thickening of the lithosphere and fast sedimentation in the pull-apart sub-basins (e.g., Horváth, 1995; Horváth et al., 2015). Neotectonics of the Pannonian Basin is characterized by tectonic inversion in the form of multi-scale folding of the lithosphere since the Late Pliocene due to the push of the Adriatic microplate in the southwest and blocking by the East European Platform in the east (e.g., Horváth and Cloetingh, 1996; Bada et al., 1999; Horváth et al., 2015).

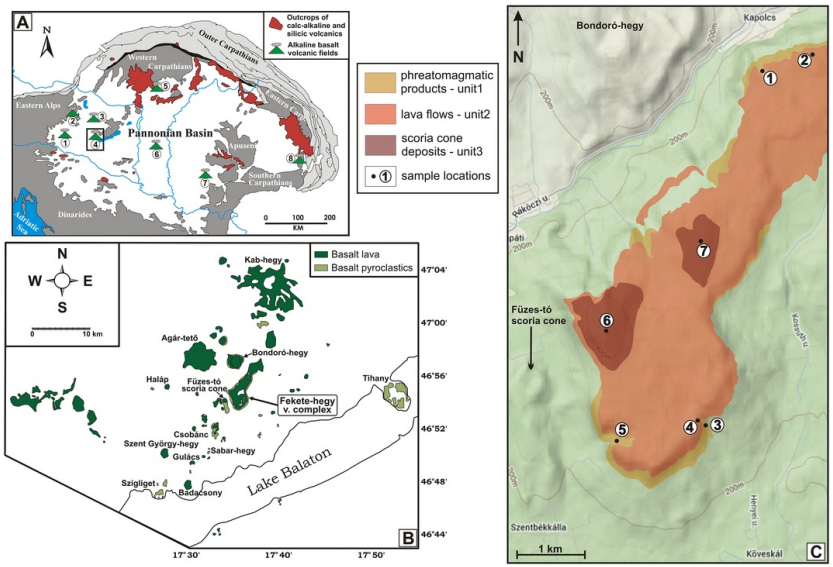

Fig. 1 (A) Geological sketch map of the Carpathian–Pannonian Region. Alkaline basaltic volcanic fields are signed with numbers: 1 – Styrian Basin; 2 – Burgenland; 3 – Little Hungarian Plain, 4 – Bakony-Balaton Highland, 5 – Štiavnica-Nógrád-Gemer, 6 – Kecel, 7 – Banat, 8 – Perşani. (B) Simplified geological map of the Bakony-Balaton Highland Volcanic Field (after Jugovics, 1968; Harangi, 2001) with the locality of the studied volcanic complex (and the names of some other eruptive centers). (C) Relief map of the Fekete-hegy volcanic complex showing the distribution of the distinct eruptive units (after Auer et al. (2007)) and the sample locations (1–7 corresponding to L1-L7 in the text) for the present study.

alt-text: Fig. 1

In the Carpathian–Pannonian Region, post-extensional alkaline basaltic volcanism took place from ~11 to ~0.11 Ma, resulting in the formation of scattered monogenetic volcanic fields mostly in the marginal areas of the region (e.g., Martin and Németh, 2004; Seghedi et al., 2004; Harangi and Lenkey, 2007). Generation of the alkaline basaltic magmas in the Pannonian Basin is connected to decompressional partial melting of the asthenosphere, however, the

geodynamic relationships of this volcanism are still controversial. Proposed models are discussed in detail by Harangi et al. (2015) (and references therein) who, in contrast to previous studies (e.g., Kovács et al., 2012), suggested that the significantly stretched Pannonian Basin (with 50–70 km lithospheric thickness in its central areas) could act as a thin-spot providing suction in the sublithospheric mantle. This could generate mantle flow from below the thick (up to 160 km) lithospheric roots of the Alps and the North European Platform resulting in the partial melting of the asthenosphere along the marginal areas of the basin.

The Bakony-Balaton Highland Volcanic Field (Fig. 1B) comprises of >50 eruptive centers which are the erosional remnants of maars, tuff rings, scoria cones, spatter cones, lava flows and shield volcanoes (e.g., Jugovics, 1968; Németh and Martin, 1999a, 1999b; Martin et al., 2003). This volcanic field is characterized by the largest amount of erupted magmas in the region, with an estimated magma productivity of 3–4 km^3 (Kereszturi et al., 2011). The volcanic activity lasted from ~8 to ~2 Ma (e.g., Balogh et al., 1986; Wijbrans et al., 2007). The whole-rock geochemistry of the majority of these alkaline basaltic volcanics as well as their xenoliths of lithospheric mantle and lower crustal origins have been extensively studied over the last decades (e.g., Embey-Isztin et al., 1989, 1990, 1993, 2001, 2003; Downes et al., 1992; Downes and Vaselli, 1995; Embey-Isztin and Dobosi, 1995; Kempton et al., 1997; Dobosi et al., 2003a, 2003b; Seghedi et al., 2004; Szabó et al., 2004; Hidas et al., 2007; Dégi et al., 2009). These studies have provided important information on the characteristics of the lithospheric mantle and lower crust, the nature of the upper mantle source and the partial melting processes beneath the area. However, little attention has been paid to the petrologic and geochemical investigation of distinct eruptive units through the succession of individual volcanic centers, as well as to the detailed mineral-scale analysis of the basaltic rocks. Despite the fact that the volcanism is essentially monogenetic, complex ascent histories have been reported for the basaltic magmas from this area and the nearby Little Hungarian Volcanic Field (Jankovics et al., 2009, 2012, 2013, 2015, 2016).

3.~~3~~ Volcanological features

The Fekete-hegy volcanic complex is a large (~12 km^2), aligned multi-vent system with a composite volcanic facies architecture resulting from contrasting eruption styles and distinct eruption episodes. The roughly NNE–SSW-trending distribution of the volcanics implies that this complex could have developed in a NNE–SSW valley system and/or been influenced by pre-existing structural elements of the same orientation (Martin et al., 2003; Martin and Németh, 2004; Auer et al., 2007). The volcanic complex consists of pyroclastic successions dominantly formed by phreatomagmatic explosive eruptions that produced at least four maars. The basal maar-forming pyroclastic units are overlain by massive lava flows (forming a capping lava plateau) and remnants of two scoria cones (Fig. 1C). These volcanics are considered here as three different eruptive units: unit 1 – phreatomagmatic products, unit 2 – lava rocks and unit 3 – scoria cone deposits that also can be considered as volcanostratigraphic units. According to Németh and Kereszturi (2015), the Fekete-hegy volcanic complex belongs to the polycyclic monogenetic volcanoes based on its complex facies architecture, similar to some other eruptive ~~centres~~ centers in the Bakony–Balaton Highland Volcanic Field (Bondoró-hegy: Kereszturi et al., 2010; Tihany: Németh et al., 2001).

Detailed descriptions and interpretations of the field relationships alongside with the documentation of the characteristics of the phreatomagmatically fragmented pyroclastic rocks are reported in detail by Auer et al. (2007). Based on their results and available geochronological data, Auer et al. (2007) concluded that the phreatomagmatic explosive activity started in the northern part of the volcanic complex, followed by effusive eruptions in the same location. A centrally located maar was formed contemporaneously or slightly later. Subsequently the volcanic activity continued mostly in the southern part of the complex with further maar-forming eruptions that were followed by lava effusion. The volcanic complex completed its activity by forming two scoria cones (in the central part) by Strombolian style explosive eruptions and intermittent Hawaiian style lava fountaining.

Only few K/Ar ages (Balogh et al., 1986) and one $^{40}Ar/^{39}Ar$ age data (Wijbrans et al., 2007) have been published for the capping lava rocks (unit 2). These results were summarized by Kereszturi et al. (2011). Although the available ages show some scatter, the time of volcanic activity can be considered to be between 3 and 4 Ma.

In this study, we have divided the volcanic activity into two main eruptive phases: the initial phreatomagmatic activity and the subsequent magmatic explosive – effusive eruptions. The formation of unit 2 (effusive) and unit 3 (explosive) can be treated as one eruptive phase after the formation of the basal maars (unit 1).

4.~~4~~ Samples and analytical methods

We performed stratigraphically controlled sampling, i.e., representative samples were collected from each of the three eruptive units. Lapillistones and lapilli tuffs from the phreatomagmatic products (unit 1) were sampled at three locations, lava rocks from the columnar and platy jointed lava flows (unit 2) at two locations, and scoria and bomb samples from the scoria cone deposits (unit 3) at two locations. The sampling sites (1–7) are shown in Fig. 1C which correspond to L1-L7 in the text.

Petrographic analyses were carried out with a Nikon YS2-T polarizing microscope and an AMRAY 1830 I/T6 scanning electron microscope at the Department of Petrology and Geochemistry, Eötvös Loránd University (Budapest, Hungary).

Whole-rock major and trace element compositions were measured at AcmeLabs (Vancouver, Canada). Major and minor elements were measured by ICP-emission spectrometry, and trace elements were determined by ICP-MS following a lithium borate fusion and dilute acid digestion.

In situ major and minor element analysis of olivine crystals and their spinel inclusions was performed with a CAMECA SX100 electron microprobe equipped with four WDS and one EDS detectors at the Department of Lithospheric Research, University of Vienna (Austria). Operating conditions were: 15 kV accelerating voltage, 25 nA beam current, 20 s counting time on peak position, focused beam diameter of 1 µm size, and PAP correction procedure for data reduction. Calibration was based on the following standards: quartz (Si), olivine (Mg), almandine (Al, Fe), wollastonite (Ca), rutile (Ti), spessartine (Mn), Mg-chromite (Cr), Ni-oxide (Ni) and apatite (P).

In the case of the phreatomagmatic products (unit 1), we also carried out olivine trace element measurements. Both single spot analyses and high-resolution crystal maps were performed by laser ablation–inductively coupled plasma–mass spectrometry (LA-ICP-MS) at the Petro-Volcanology Research Group (PVRG) facility, Department of Physics and Geology, University of Perugia (Italy). We used a Teledyne Photon Machine G2 laser ablation system coupled to a Thermo Fisher Scientific iCAP-Q ICP-MS. Helium was utilized as carrier gas with Ar and N_2 added just after the ablation cell to avoid plasma destabilization and heighten the instrumental sensitivity, respectively.

Single spot measurements were carried out on the cores, growth zones and rims of olivine crystals showing diverse textures, zoning patterns and compositions. Data were collected for Li, Na, Al, P, Ca, Sc, Ti, V, Cr, Mn, Co, Ni, Zn, Y, Zr and Nb, using spot sizes of 15 and 25 µm, depending on the size of the cores and on the width of the zones and rims being analyzed, with a repetition rate and fluence of 8 Hz and 3.5 J/cm^2, respectively. Dwell times were 10 ms per analyte. The NIST 610 reference material was used as the calibration standard, and USGS BCR2G glass was our quality control. Si concentrations determined by EMPA were used as an internal standard. Data Reduction was carried out using the "Trace_Elements" Data Reduction Scheme of the Iolite v.3 software package (Paton et al., 2011). Under the reported analytical conditions, precision and accuracy are typically better than 10% (Petrelli et al., 2008, 2016). Repeated analyses (n = 10) of the USGS BCR2G reference material performed in the same analytical session of the data reported in present study confirmed the expected figures of merits with the only slight deviations of Cr and P, showing divergences from the reference values of 11 and 13 %, respectively (Supplementary Table 5).

Fifteen representative olivines were imaged following the line rastering technique proposed by Ubide et al. (2015) to produce multi-elemental crystal maps. Crystals were pre-ablated before mapping (as suggested by Kahl et al. (2017)), using a spot size of 100 µm, repetition rate of 20 Hz and fluence of 2.5 J/cm^2. A range of spot sizes (5, 8, 12 and 15 µm) and scan speeds (2, 4, 5 and 7 µm/s) was implemented depending on the size of the area being mapped. Repetition rate and fluence were fixed at 8 Hz and 3.5 J/cm^2, respectively. Crystal maps were produced using the Iolite module "Images from selections" and additional transects were created using CellSpace (Paul et al., 2012). Average compositional data from crystal zones were extracted using Monocle (Petrus et al., 2017) for further investigation of compositional relationships.

5.5 ~~5~~ General petrology

5.1.~~5.1~~ Petrographic characterization

The lapillistones and lapilli tuffs representing the phreatomagmatic products of unit 1 are characterized by varied textural and componentry appearances. As juvenile pyroclasts they contain sideromelane and tachylite glass shards (≤ 3 mm) and lapilli- and bomb-sized (0.2–15 cm) basalt fragments. The glass shards have variable vesicularity and crystal content. The basalt fragments show medium to highly vesicular, porphyritic textures. The accidental lithics (~0.1–10 cm) include by peridotite, limestone, sandstone, phyllite, siltstone and mudstone. Amphibole, clinopyroxene (colorless and green under the optical microscope), olivine, orthopyroxene and quartz occur as dispersed crystals and crystal fragments (≤ 1.5 mm) in the deposits.

The juvenile pyroclasts contain a remarkably diverse mineral assemblage (≤ 4 mm-sized crystals) of olivine + clinopyroxene + orthopyroxene + spinel + amphibole + quartz + K-feldspar ± plagioclase. In addition, they also comprise various xenoliths (≤ 7 mm) of peridotite, sandstone, siltstone and mudstone (Fig. 2A–B). The minerals recognized in the juvenile pyroclasts show highly variable appearances with a significant amount of crystals showing disequilibrium textures (Supplementary Fig. 1): rounded and embayed olivines with diffuse rims; anhedral and ragged orthopyroxenes with fine-grained reaction rims; subhedral clinopyroxenes with variably resorbed, colorless (under the optical microscope) cores (often with spongy parts) and pale brown, sector zoned rims; anhedral and rounded spinels with spongy rims; ragged and anhedral amphiboles often with reaction rims. All these textural features suggest a xenocrystic origin for these minerals (olivines, orthopyroxenes, spinels, amphiboles and rounded clinopyroxene cores) which are originated from the subcontinental lithospheric mantle (together with the peridotite xenoliths). Very similar mineral assemblages characterized by the same disequilibrium textures were reported from the alkaline basalts of the adjacent Füzes-tó scoria cone and Bondoró-hegy eruptive centers (Fig. 1B), where these anhedral olivines, orthopyroxenes, spinels and colorless clinopyroxene cores were proved to be lithospheric mantle-derived xenocrysts based on their textures and compositions (Jankovics et al., 2009, 2013, 2016). The Fekete-hegy samples contain anhedral, resorbed quartz and K-feldspar crystals, which are interpreted as xenocrysts derived from the crust (together with the siliciclastic xenoliths). Glomerocrysts of olivine and/or clinopyroxene are often observed. The microphenocrysts (≤ 150 µm) in the juvenile components are olivine, clinopyroxene, plagioclase and Fe-Ti-oxides, and the groundmass consists of the same mineral phases with the addition of a small amount of glass.

Some differences can be observed in the phreatomagmatic products between the three sample locations (L1, L3 and L5) (Fig. 1C). For example, they differ in abundance and type of lithic fragments, the appearance and size of the sideromelane glass shards, and the amount of the xenocrysts in the juvenile pyroclasts. In addition, at sample location 1 (L1) the deposits contain abundant megacrysts (0.5–3 cm) of amphibole >>> clinopyroxene >>> mica, which are present as independent pyroclasts as well as inside the juvenile basalt fragments. Compared to L1 and L3, the juvenile basalt fragments from L5 comprise the largest amount of crustal siliciclastic xenoliths which show textural features resulting from partial melting by the host basaltic magma (Supplementary Fig. 1A).

In contrast to the juvenile pyroclasts of the phreatomagmatic eruptive products (unit 1), the lavas of unit 2 are less complex, with non-vesicular, porphyritic textures, only comprised of olivine ~~≫~~ clinopyroxene > plagioclase phenocrysts (Fig. 2C). Olivines and/or clinopyroxenes often form glomerocrysts. In rare cases, they contain a few anhedral xenocrysts of olivine and orthopyroxene as well as sparse sandstone xenoliths. The microphenocrysts are olivine, clinopyroxene, plagioclase and Fe-Ti-oxides, and the groundmass consists of the same mineral assemblage with the addition of apatite microlites. There are no significant textural differences between the lavas of L2 and L4.

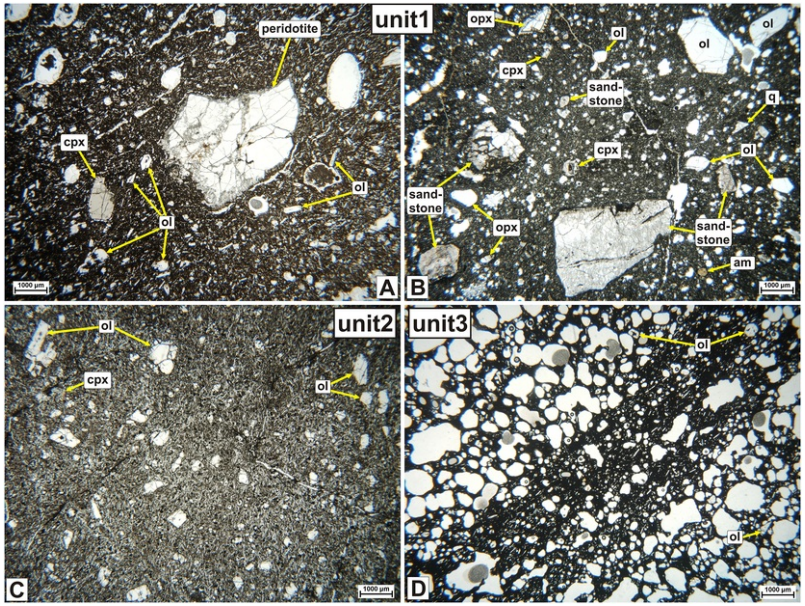

Fig. 2 General petrographic features of the studied samples (photomicrographs, PPL). (A, B) Juvenile basalt fragments from the phreatomagmatic eruption products of unit 1 (from L1 and L5, respectively) with a diverse mineral assemblage (olivine, clinopyroxene, orthopyroxene, amphibole, spinel, quartz) and various xenoliths (e.g., peridotite, sandstone). (C) Columnar jointed lava sample from unit 2 containing only olivine and minor clinopyroxene phenocrysts. (D) Scoria sample from unit 3 only with olivine phenocrysts. Ol – olivine, cpx – clinopyroxene, opx orthopyroxene, am – amphibole, q – quartz.

alt-text: Fig. 2

The scoria and volcanic bomb samples of unit 3 are defined by the same characteristics of the lavas. They show medium – highly vesicular, porphyritic textures containing only olivine (often partially iddingsitised) ~~≫~~ plagioclase > clinopyroxene phenocrysts (Fig. 2D). Sparse rounded olivine xenocrysts and siliciclastic xenoliths are also present. The microphenocrysts and groundmass are characterized by the same mineral phases as described in the lava samples, with the addition of some glass in the matrix. No considerable textural differences are observed between the scoria cone deposits from L6 and L7.

The very similar petrographic features of the basaltic rocks from unit 2 and unit 3 supports the decision to treat them together as the same eruptive phase, thus they can interchangeably be referred to as unit 2-3.

It can be concluded that within the studied monogenetic volcanic complex the eruptive units represent different petrographic types of small-volume basalts: unit 1 samples are characterized by a complex petrography, ~~whilst~~ while unit 2-3 samples represent petrographically simple basaltic volcanics.

5.2.~~5.2~~ Whole-rock geochemistry

Previous whole-rock geochemical data from the northern and southern effusive rocks, as well as one of the scoria cones (corresponding to our L6) of the Fekete-hegy volcanic complex were reported by Jugovics (1976) and Embey-Isztin et al. (1993). For this study, with the exception of L3 where the juvenile basalt fragments are more altered, samples were analyzed from each of the studied sample localities (Fig. 1C): juvenile basalt fragments from the lapillistones and lapilli tuffs (unit 1), lavas (unit 2), scoria and volcanic bombs (unit 3). New whole-rock compositions are given in Supplementary Table 1.

The studied samples show basanitic, trachybasaltic and basaltic compositions based on their SiO_2 and total alkali contents (Fig. 3A). Their Mg# ($Mg/(Mg + Fe^{2+})$) ranges from 0.55 to 0.72. The juvenile basalt fragments from L1 and L5 have Mg# 0.66-0.68 and 0.72, respectively. The lava from L2 is characterized by a higher Mg# (0.67) than that of L4 (0.64). The lowest Mg# values are found in the scoria cone deposits: 0.56-0.63 (L6) and 0.55 (L7). All

samples have very similar, steep chondrite-normalized REE patterns, which are characteristic for basalt compositions in intraplate settings (Fig. 3B).

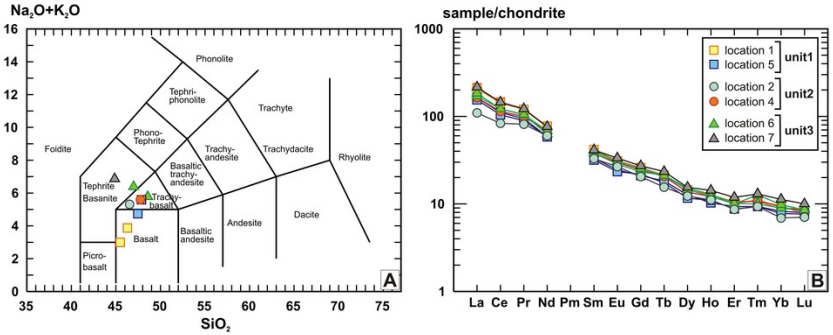

Fig. 3 Whole-rock compositions of the Fekete-hegy samples from the three eruptive units (from all studied localities with the exception of L3). (A) TAS diagram (after Le Bas et al., 1986). (B) Chondrite-normalized (Nakamura, 1974) REE variation plot. Locations 1–7 correspond to L1-L7 in the text.

alt-text: Fig. 3

6.6 Olivine textures, zoning and compositions

Aside from the striking differences observed between the appearance and modal mineralogy of the basaltic rocks from unit 1 and unit 2–3, there are also significant distinctions between the textures, zoning and chemistry of their olivine crystals. While the olivines in unit 1 show a remarkably large diversity, the olivines of unit 2 and unit 3 are simple and uniform. Olivine compositions measured from all the three eruptive units are plotted in Fig. 4A–B, and representative major and trace element compositions are given in Table 1. The complete olivine dataset is available in Supplementary Tables 2 and 3.

6.1.6.1 Zoning patterns and major element variations

In the juvenile pyroclasts (sideromelane and tachylite glass shards, lapilli- and bomb-sized basalt fragments) of the phreatomagmatic products, olivine ranges from euhedral to anhedral in shape, with various zoning patterns (Fig. 5) accompanied by a large compositional variety (Fig. 7). Five different olivine zoning types can be distinguished, and are characterized by the following features:

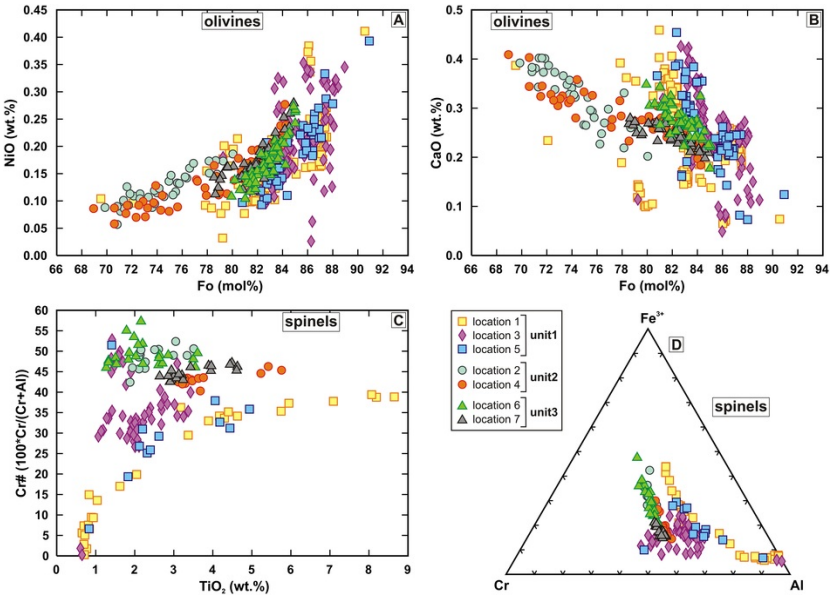

Fig. 4 Compositions of the studied olivine crystals and their spinel inclusions from the three eruptive units (L1-L7 samples). (A) Fo (mol%) vs. NiO (wt.%) and (B) Fo (mol%) vs. CaO (wt.%) plots of olivines. (C) TiO_2 (wt.%) vs. Cr# ($100 * Cr/(Cr+Al)$) and (D) Cr-Al-Fe^{3+} diagrams of spinels.

alt-text: Fig. 4

Table 1 Representative major (wt.%) and trace element (ppm) compositions of the studied olivine crystals from the three eruptive units.

alt-text: Table 1 (Please insert narrow blank columns between the compositions of the different olivine types (in order to make the table more clear for the readers).)

	Type I olivine	-	-	-	-	-	Type II olivine	-	-	-	-	-	Type III olivine	-	-	-	-	-	-	-	-	Type IV olivine		
	Core	Rim	Core	Rim	Core	Rim	Core	Rim	Core	Rim	Core	Rim	Core	Growth zone	Rim	Core	Growth zone	Rim	Core	Growth zone	Rim	Core	Rim	C
	ol2_2	ol2_3	ol3_1	ol3_3	ol4_1	ol4_4	ol35_1	ol35_2	ol37_1	ol37_2	ol39_1	ol39_2	ol61_1	ol61_2	ol61_3	ol62_1	ol62_2	ol62_3	ol66_1	ol66_2	ol66_3	ol81_2	ol81_3	o
Eruptive unit	Unit1	Unit1	Unit1	Unit1	Unit1	Unit1	Unit1	Unit1	Unit1	Unit1	Unit1	Unit1	Unit1	Unit1	Unit1	Unit1	Unit1	Unit1	Unit1	Unit1	Unit1	Unit1	Unit1	U
Sample location	L1	L1	L5	L5	L5	L5	L1	L1	L1	L1	L1	L1	L1	L1	L1	L5	L5	L5	L1	L1	L1	L1	L1	
SiO_2	40.14	39.44	39.65	39.60	40.06	39.36	39.33	39.11	39.78	39.36	39.59	39.35	39.26	39.94	39.14	39.38	39.95	39.57	39.68	40.32	39.27	38.70	39.27	3
TiO_2	0.04	0.07	0.03	0.03	0.02	0.06	0.04	0.03	0.04	0.04	0.04	0.04	0.04	0.03	0.03	0.02	0.04	0.03	0.03	0.01	0.03	0.03	0.04	0.
Al_2O_3	0.02	0.00	0.04	0.05	0.04	0.03	0.03	0.03	0.02	0.04	0.04	0.03	0.03	0.03	0.00	0.04	0.00	0.01	0.04	0.04	0.03	0.02	0.02	0.
FeO	12.48	16.31	12.93	14.68	12.42	16.10	16.76	17.33	15.54	16.58	15.98	16.04	15.99	12.16	16.50	16.27	13.91	15.80	15.83	12.35	16.38	19.26	16.05	1
MnO	0.22	0.27	0.194	0.284	0.169	0.276	0.293	0.327	0.236	0.280	0.244	0.257	0.20	0.21	0.30	0.20	0.23	0.26	0.191	0.209	0.279	0.24	0.24	0.
MgO	46.91	43.46	45.83	44.44	46.30	43.41	42.89	42.34	43.81	42.63	43.44	43.67	44.46	46.93	43.70	43.80	45.67	44.20	43.85	46.33	43.13	41.80	44.05	4
CaO	0.22	0.27	0.143	0.355	0.218	0.273	0.322	0.372	0.231	0.279	0.219	0.247	0.19	0.22	0.30	0.16	0.24	0.28	0.175	0.217	0.290	0.13	0.27	0.
Cr_2O_3	0.04	0.00	0.02	0.02	0.04	0.01	0.02	0.03	0.02	0.01	0.04	0.03	0.02	0.02	0.04	0.01	0.03	0.02	0.02	0.02	0.00	0.00	0.01	0.
NiO	0.22	0.12	0.227	0.110	0.215	0.153	0.105	0.098	0.205	0.138	0.184	0.143	0.20	0.22	0.13	0.15	0.22	0.18	0.170	0.231	0.128	0.09	0.17	0.
P_2O_5	0.11	0.06	0.101	0.041	0.000	0.008	0.025	0.032	0.057	0.025	0.043	0.014	0.00	0.03	0.05	0.08	0.05	0.01	0.005	0.022	0.027	0.07	0.10	0.
Total	100.39	100.01	99.16	99.59	99.48	99.67	99.81	99.68	99.94	99.38	99.82	99.81	100.39	99.79	100.17	100.10	100.33	100.36	99.98	99.76	99.55	100.35	100.23	1
Fo	87.02	82.60	86.34	84.37	86.92	82.77	82.02	81.33	83.40	82.08	82.89	82.91	83.21	87.31	82.52	82.75	85.41	83.29	83.16	86.99	82.44	79.46	83.02	7
Li	2.12	3.49	2.95	3.2	1.97	2.68	3.01	3.1		2.88	3.1	3.3	1.89	2.27	3.61	2.02	3.7	3.3	2.59	2.43	3.92	2.91	3.7	
Na	91.4	92	73.6	103	88.6	113	75.2			87	83	74	77.8	96	70	82.4	92	71	62.6	81	58		58	
Al	256.2	167.7	218.5	178.7	240.8	216	183.2	170.2		164.6	239	303	288.6	233.4	175.6	310.6	190.4	198	276.6	301	206	340	319	
P	181	169	302	202	106.2	144	155.3	118		187	182	187	61.7	222	156	56.3	186	105	106.6	191	176.2	108	179	
Ca	1433	1360	738	2290	1514	1920	1522	2360		1560	1310	2370	1066	1380	1370	1073	1720	1560	1078	1520	1930	940	2270	
Sc	8.87	8.45	7.25	10.4	8.58	10.37	7.9	9.7		8	7.41	9.3	8.47	10.55	10.6	8.29	10.49	9.5	7.02	9.36	8.9	7	9.3	
Ti	108.9	81.5	101.2	114	99.5	114	87.3	132		93.8	91.6	129	101.2	92.3	111.4	103.7	104	103	96.4	108.6	129	134	173	
V	5.71	3.79	7.26	3.31	5.38	4.14	3.87	3.99		4.09	4.9	4.26	7.54	4.72	3.79	6.78	5.19	4.74	23.2	5.74	4.37	20.7	6.1	
Cr	120.1	81.2	155	80.4	161.8	80.8	85	48.9		80.9	79.7	77	13.2	136.6	85	8.5	146.2	129	50.7	124.9	101		240	

Mn	1553	1950	1690	2275	1527	2158	1895	2700		2040	1903	2430	1557	1560	2035	1647	1969	2027	1476	1691	2220	1954	2468	
Co	153.6	165.2	133.3	151.2	149.1	163.8	156.1	168.9		162.9	163.2	166.3	176	146.5	156.9	179.9	157.5	151.3	175.8	153.4	154	202	157.3	
Ni	1808	1255	1911	983	1562	1097	1308	764		1218	1432	931	1557	2042	1163	1087	1446	1417	1358	1808	1041	437	821	
Zn	95.3	158	112.8	152	97.6	150.9	128.9	167		155.1	140	160	119.8	102.5	157.3	136.7	150.2	135	124	106.7	145	197	165	
Y	0.083	0.094	0.086	0.069	0.047	0.165	0.083	0.146		0.073	0.075	0.174	0.062	0.101	0.108	0.054	0.098	0.084	0.101	0.097	0.145	0.172	0.18	
Zr	0.219	0.099	0.059	0.15	0.05	0.152	0.054	0.079		0.051	0.17	0.42	0.051	0.154	0.131	0.082	0.068	0.1	0.442	0.71		0.87	0.19	
Nb	0.191	0.064	-	-	-	0.019	-	-	-	-	0.025	0.26	-	-	-	-	-	-	0.584	0.92	0.061	1.39	0.201	-

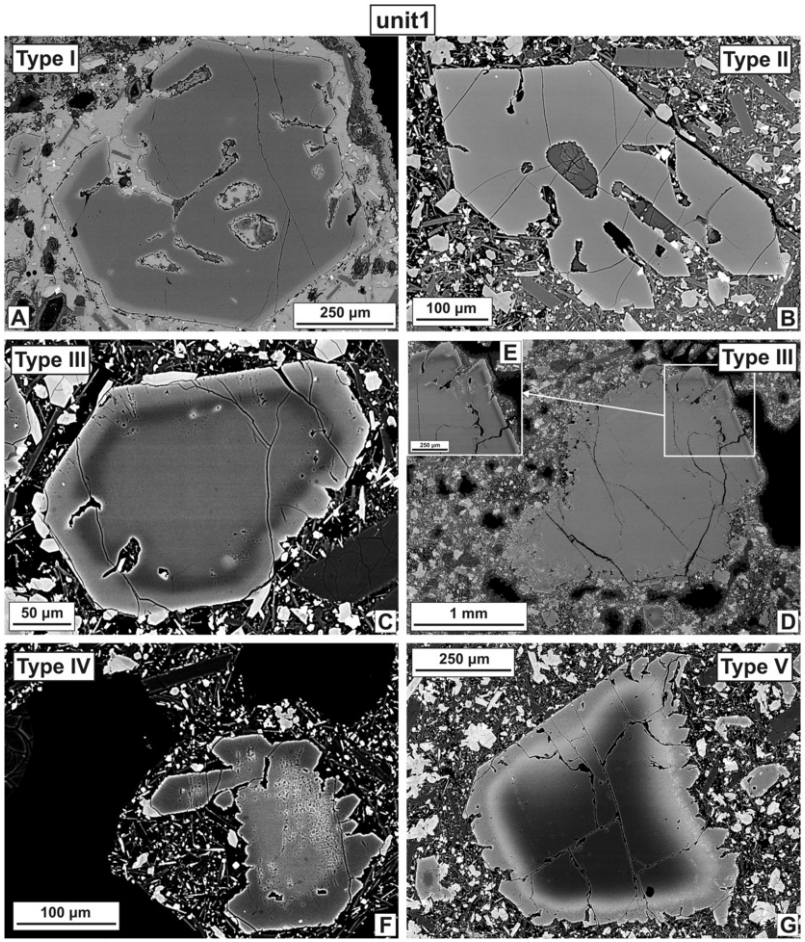

Fig. 5 Textural and zoning characteristics of the various olivine populations from the unit 1 samples (BSE images). (A) Skeletal type I olivine with normal, single step zoning; euhedral core and rim. (B) Skeletal type II olivine with normal, progressive zoning. (C) Type III olivine with multiple (reverse to normal), double step zoning; subhedral core, growth zone and rim. (D) Large type III olivine with an anhedral, fragmented core (subgrains on its left side), surrounded by a euhedral growth zone and rim, enlarged in (E). (F) Type IV olivine with reverse, single ste zoning; the anhedral core is overgrown by a skeletal rim. (G) Type V olivine with multiple (normal to reverse), double step zoning; anhedral core, followed by a rounded growth zone and a skeletal rim.

alt-text: Fig. 5

Type I olivine – normal, single step zoning (Fig. 5A): one of the most abundant zoning types, crystals range in size from 70 to 1500 µm, and are mainly skeletal, euhedral-subhedral in shape. Cores are mostly euhedral-subhedral (rarely anhedral) and have high Fo contents (Fo_{85-89}), while rims have lower Fo (Fo_{81-85}). The compositional change from the crystal core to the rim is usually sharp, and therefore defined as single step zoning. Occasionally, however, some crystals display a more gradual core-rim transition. Compared to the rims, cores are lower in CaO and MnO, and similar in NiO. One of the type I olivine cores separates from the others due to higher Fo and NiO contents (Fig. 7A).

Type II olivine – normal, progressive zoning (Fig. 5B): this population is as abundant as type I olivines. Crystals are euhedral-subhedral, predominantly skeletal (50–700 µm). These olivines show continuously changing compositions representing mild, progressive zoning: decreasing Fo (from Fo_{85} to Fo_{81}) and NiO, and increasing CaO and MnO concentrations from their cores to the rims (Fig. 7A–C).

Type III olivine – multiple (reverse to normal), double step zoning (Fig. 5C–E): euhedral-subhedral, often skeletal crystals, with a wide range of sizes (100–4500 µm). This zoning type has the same frequency as the type I and II olivines. These crystals consist of subhedral-anhedral, often rounded, Fo_{83-85} cores mantled by a Fo_{85-88} growth zone, with an often skeletal, Fo_{81-84} rim (Fig. 7). Fo-rich growth zones have variable forms: usually skeletal in appearance; constant or varying thickness through a given crystal; regular or irregular contour; not always continuous through the entire crystal. Both zone boundaries (i.e., between the core and the growth zone and between the growth zone and the rim) are sharp, representing abrupt compositional changes. This zoning type can therefore be considered as a “double” step zoning. It is worth noting that the growth zone and the rim together display the same overall appearance and composition as the core and rim of the type I olivine crystals.

Type IV olivine – reverse, single step zoning (Fig. 5F): the least abundant zoning type, crystals are comparably smaller (90–400 µm) and euhedral-subhedral. Cores are anhedral and rounded showing lower Fo (Fo_{79-80}) and CaO, variable NiO and similar MnO, compared to the frequently skeletal rims (Fo_{82-83}) (Fig. 7A–C).

Type V olivine – multiple (normal to reverse), double step zoning (Fig. 5G): this is also a sparse population with subhedral to anhedral olivines (260–2100 µm). Crystal cores are anhedral and rounded with higher Fo (Fo_{83-91}) and NiO, and lower CaO and MnO compared to the surrounding rounded growth zone (with constant thickness; Fo_{70-80}) and the often skeletal outermost rim (Fo_{78-84}) (Fig. 7A–C).

Aside from the five different olivine types, we also observed a crystal clot (500 µm in size) of olivines in a sideromelane glass shard (Fig. 9D). These olivine crystals are euhedral-subhedral and range between 20 and 100 µm in size. They show weak progressive normal zoning and coexist with spinel crystals (they are attached to, or partly or entirely included by the olivines). Their compositions vary in a restricted range (e.g., Fo_{86-88}) (Fig. 7A–C).

The large variability in shape, texture, zoning appearance and composition of the olivine crystals in the unit 1 samples is not only observed throughout the entire olivine assemblage but also within the individual olivine types (this is particularly characteristic of the type V crystals). All five olivine types occur in the phreatomagmatic products from each of the three studied sample localities (L1, L3 and L5).

In contrast, the euhedral-subhedral, occasionally skeletal olivine crystals of the lavas (unit 2), scoria and volcanic bombs (unit 3) are always normally zoned (progressive zoning) (Fig. 6) and do not show the variety of zoning patterns observed in olivines from the phreatomagmatic products. This simple progressive zoning is defined by gradual, rather than abrupt, core-to-rim variation in major elements: decreasing Fo and Ni, increasing Ca and Mn (Fig. 4A–B).

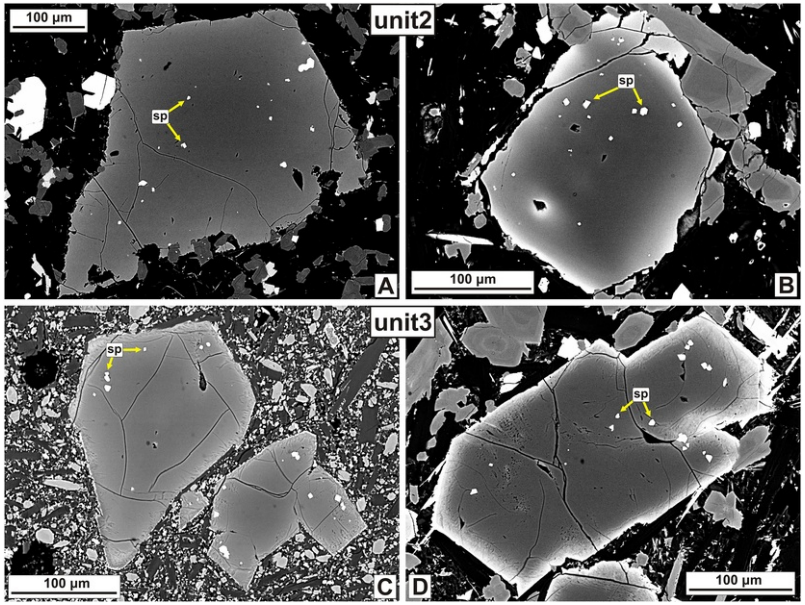

Fig. 6 Olivine crystals from the unit 2 and 3 samples (BSE images): they are uniform, characterized by simple progressive normal zoning and frequently contain spinel (sp) inclusions throughout. Subhedral olivines in (A) L2 and (B) L4 unit 2 lavas, and from (C) L6 and (D) L7 unit 3 scoria cone deposits.

alt-text: Fig. 6

The lava samples from unit 2 show some differences between sampling localities. Lava-hosted olivines from L2 have lower Fo ($Fo_{70–80}$) and NiO contents than those from L4 ($Fo_{69–84}$). However, they contain similar concentrations of CaO and MnO (Fig. 4A–B).

Olivines from unit 3 scoria and volcanic bombs are characterized by very similar compositions. For example, the scoria from L6 comprises olivines with $Fo_{80–85}$, and the olivines of L7 contain $Fo_{79–85}$ (Fig. 4A–B).

6.2.~~6.2~~ Trace element characteristics

In addition to major element analyses, trace element measurements were also carried out for each of the olivine populations from unit 1. Major and trace element analyses show a good agreement between Ni, Ca and Mn data. Plots of Fig. 7D–H show the trace element variations for the olivine single spot measurements as a function of their Fo contents. There are no clear correlations between Fo and trace elements in either the individual olivine types, or the entire olivine dataset, however there are definite relationships between cores, growth zones and rims of each olivine population. The cores of type I olivines have the highest Fo contents but cover a range of trace element concentrations, e.g., ~50–190 ppm Cr and ~60–300 ppm P. Type II cores have a more constrained range of trace element concentrations, e.g., ~60–90 ppm Cr and 130–150 ppm Zn. Type III olivine cores are generally characterized by lower values of Cr and P than those of type I and II (~10–50 ppm and ~60–110 ppm, respectively) and higher Co (~170–180 ppm). Type III growth zone compositions consistently overlap with type I cores. Type IV olivine cores have lower Cr (~0–60 ppm) and higher Zn (~170–300 ppm) concentrations compared to the type II olivines and all crystal rims. Type V cores tend to yield a wide variation of compositions, with the exception of Cr and P which occupy a low, restricted range of concentrations, ~20–30 ppm and ~70–90 ppm, respectively. Type V growth zones are very similar in composition to type IV cores. Rim compositions for all olivine types generally overlap, in both Fo content and trace element concentration. Rims are also consistent in composition with type II cores (Fig. 7D–H).

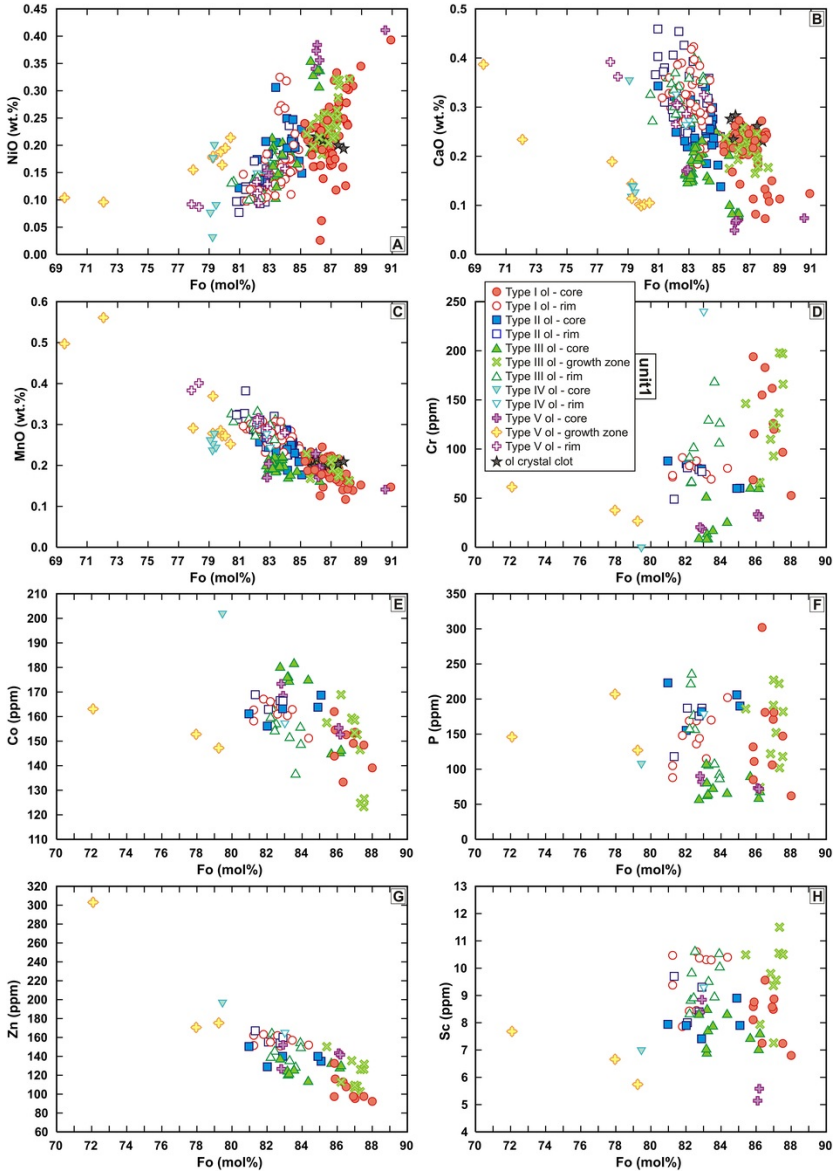

Fig. 7 (A-C) Major and (D-H) trace element compositional variations against Fo (mol%) content in the different olivine populations from the phreatomagmatic unit 1 samples. Major elements are in wt.%, trace elements are in ppm.

alt-text: Fig. 7

Trace element maps displaying intra-crystal compositional variations for each olivine type are presented in Fig. 8. The different zoning patterns shown in the BSE images (Figs. 5, 8) and described above for each olivine type (Fig. 7) are clearly reproduced in the high-resolution trace element crystal maps. The maps illustrate that the intra-crystal compositional changes of trace elements Ni, Cr, Mn and Zn mostly correlate with Fo contents. Ni and Fo variations correlate positively across olivine types I, II, III and V, but show negative correlation in the representative type IV crystal (Fig. 8D). Cr correlates positively with Fo across the type I, II, III and IV crystals, however this is not the case in the type V olivines. The representative type V crystal map (Fig. 8E) shows that both the core and the growth zone (which significantly differ in Fo; Figs. 6–7) have the same, low-Cr concentrations surrounded by a Cr-richer

rim. The other mapped type V crystal (Fig. 5G, Supplementary Fig. 2), however, displays a growth zone that is poorer in Cr than the core (corresponding to the Fo variation) and it is followed by a Cr-richer rim. Mn and Zn behave similarly and show negative correlation with Fo in all olivine types excepting the type IV crystal where these two elements change oppositely (Mn correlates positively but Zn negatively with Fo).

Co, P, Sc, V and Ti have relatively homogeneous concentrations across all crystals and do not mirror the zoning observed for Fo, Ni, Cr, Mn, Zn, nor any additional zoning features. In the case of type III olivines, however, the crystal cores display a slight enrichment in Co and a slight depletion in P compared to their growth zones and rims. Additionally, the slight depletion in P can be also detected in type V crystals.

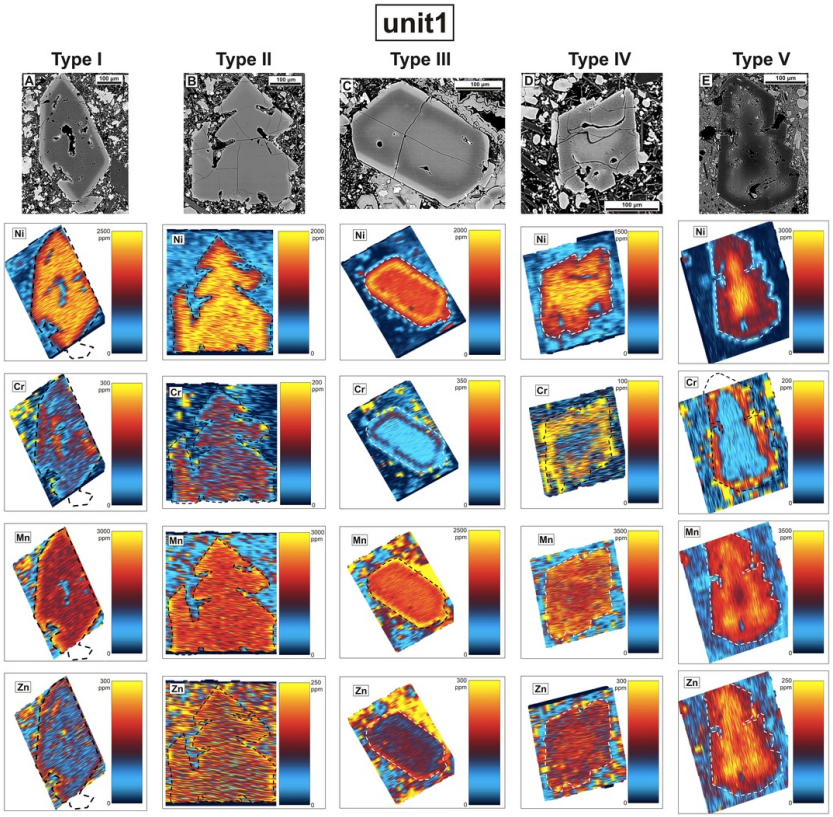

Fig. 8 High-resolution LA-ICP-MS trace element crystal maps (Ni, Cr, Mn and Zn) and corresponding BSE images of the different olivine types from the phreatomagmatic unit 1 samples.

alt-text: Fig. 8

7.~~7~~ Spinel occurrence and chemistry

Spinel occurs as inclusions in olivines in the studied rocks of each eruptive unit (Figs. 4, 5, 8 and 9). Spinel compositions measured from all the three units are plotted in Fig. 4C–D and representative compositions are shown in Table 2. The spinels are euhedral to subhedral crystals with a homogeneous interior (no zoning), ranging in size between 1 and 20 µm.

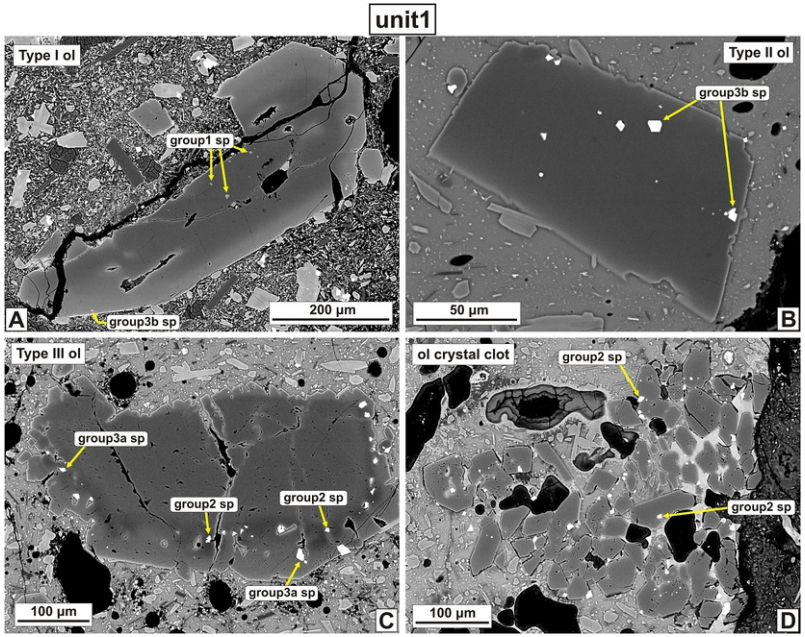

Fig. 9 Occurrence (BSE images) and chemistry of olivine-hosted spinel inclusions from the phreatomagmatic unit 1 samples. Spinels usually occur (A) in the cores of type I olivines, (B) in various portions of type II olivines, (C) in the growth zones and rims o type III olivines, and (D) in the studied olivine crystal clot.

alt-text: Fig. 9

Table 2 Representative analyses of the studied olivine-hosted spinel inclusions from the three eruptive units.

alt-text: Tabl (Please insert narrow blank columns between the compositions of the different spinel groups (in order to make the table more clear for the readers).)e 2

-	Group1 spinel	-	-	Group2 spinel	-	-	Group 3a spinel	Group3b spinel		~Group2 spinel	-	-	-
	sp1	sp4	sp9	sp22	sp24	sp27	sp74	sp38	sp82	sp95	sp124	sp142	sp150
Host olivine	Type ~~ii~~III	Type ~~i~~I	Type ~~i~~I	In ol crystal clot	Type ~~ii~~III	Type ~~ii~~III	Type ~~ii~~III	Type ~~i~~I	Type ~~i~~I	Progressive normal	Progressive normal	Progressive normal	Progressive normal
sp position in ol	In the growth zone	In the core	In the core	Attached to olivine	In the growth zone	In the growth zone	In the growth zone	In the rim	In the rim	In the core	In the core	In the core	In the core
Eruptive unit	Unit1	Unit1	Unit1	Unit1	Unit1	Unit1	Unit1	Unit1	Unit1	Unit2	Unit2	Unit3	Unit3
Sample location	L1	L1	L1	L3	L3	L5	L3	L1	L3	L2	L4	L6	L7
SiO_2	0.23	0.27	0.17	0.18	0.16	0.20	0.14	0.17	0.14	0.10	0.12	0.10	0.11
TiO_2	0.77	0.72	0.94	1.40	1.40	1.41	1.14	5.95	3.25	2.27	3.27	1.33	2.96
Al_2O_3	58.50	57.13	52.86	23.04	27.09	22.96	34.75	18.08	25.21	18.27	22.65	20.11	23.33
Fe_2O_3	7.79	6.77	7.23	10.70	6.90	8.19	9.71	23.25	18.28	20.14	13.67	18.63	12.26
FeO	11.49	9.56	10.96	19.95	16.53	15.19	15.86	24.91	19.02	25.06	22.10	21.46	20.39

MnO	0.10	0.11	0.12	0.32	0.23	0.17	0.24	0.32	0.26	0.31	0.27	0.31	0.24
MgO	19.96	21.03	19.65	10.34	13.24	13.73	14.39	9.23	12.18	6.90	10.07	8.94	11.22
Cr_2O_3	1.53	4.55	8.10	32.02	32.91	36.35	22.69	16.04	19.39	24.51	25.85	26.87	28.08
NiO	0.19	0.21	0.26	0.11	0.25	0.17	0.19	0.12	0.14	0.16	0.16	0.14	0.14
Total	100.57	100.45	100.34	98.38	98.88	98.40	99.12	98.24	98.13	97.96	98.42	98.10	98.92
Cr#	1.72	5.07	9.32	48.25	44.91	51.51	30.46	37.30	34.04	47.3~~69~~17	43.36~~01~~	47.2~~64~~87	44.6~~69~~17
Mg#	0.76	0.80	0.76	0.48	0.59	0.62	0.62	0.40	0.53	0.3~~29~~13	0.4~~48~~15	0.4~~26~~13	0.~~495~~150

Fe_2O_3 is calculated on the basis of stoichiometry; Mg# = Mg / (Mg + Fe^{2+}); Cr# = 100 * Cr / (Cr + Al).

In the phreatomagmatic unit 1, spinels are found as inclusions in discrete portions of the different olivine types: in the cores and rims of type I, in all parts of type II, in the growth zones and rims of type III (only one type III crystal was found containing spinels in its core as well), in the rims of type IV and in the rims of type V olivines (Figs. 5, 8 and 9). Spinel inclusions (1–14 µm in size) were additionally observed in the studied olivine crystal clot where they are attached to or partly or entirely encapsulated by the olivines (Fig. 9D). Unit 1 spinels show a similarly large compositional diversity to the unit 1 olivines and they can be divided into three major groups (Fig. 10A). Group 1 spinels are characterized by low Cr-numbers (Cr#; 100 * Cr/(Cr + Al)) between 0.24 and14.9 and low TiO_2 (0.61–1 wt.%). They occur mainly in type I olivine cores and occasionally in the growth zones of type III olivines (there are some rare occurrences of group 1 spinels in type II and type III crystal cores). Group 2 spinels, present in the olivine crystal clot (Fig. 9D) and growth zones of type III olivines, have relatively high Cr# (41.8–52.8) and a slightly larger range in TiO_2 contents (1.4–3.1 wt.%). Group 3 spinels, the most dominant spinel group, are defined by moderate Cr# (25.1–40.5) in comparison to group 1 and 2, and variable TiO_2 concentrations ranging from 1.1 to 8.7 wt.%. They occur in type II olivine cores and in all olivine rims. Rarely, group 3 spinels are found in type III olivine growth zones. Group 3 spinels are divided into two subgroups based on their TiO_2 contents: group 3a comprises the lower-TiO_2 (<~2 wt.%) spinels, ~~whilst~~ while group 3b represents those with >~2 wt.% TiO_2 concentrations (the majority of the group 3 spinels belongs to the latter subgroup). Additionally, there are some spinel inclusions that show transitional compositions (17–19.9 Cr#, 1.6–2.1 wt.% TiO_2) between the group 1 and 3 spinels. Group 1 and 3 spinels occur in the phreatomagmatic deposits from all three of the investigated sample locations, whereas group 2 spinels are only present in samples from L3 and L5.

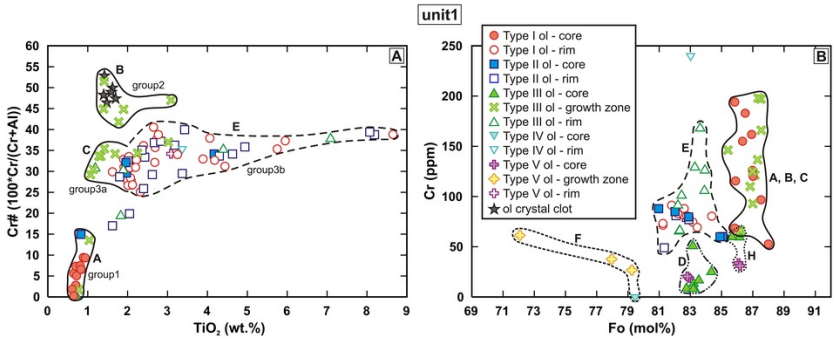

Fig. 10 (A) Plot of TiO_2 (wt.%) vs. Cr# (100 * Cr / (Cr + Al)) of the studied spinels showing their distinct compositional groups as well as grouping of the defined magmatic environments in the (A) spinel (TiO_2 vs. Cr#) and (B) olivine (Fo vs. Cr) chemical space (phreatomagmatic eruptive phase – unit1). Symbols are as in Fig. 7.

alt-text: Fig. 10

The simple normally zoned olivine crystals from the later magmatic explosive – effusive eruption products (unit 2–3) contain spinel inclusions throughout, and these inclusions frequently occur as clusters or chains (Fig. 6). Compared to the spinels found in unit 1 samples, the spinels in unit 2–3 samples show a restricted range of compositions (Fig. 4C–D) and they can be grouped together. The lavas from unit 2 contain spinels with slightly different compositions: L2 spinel inclusions have 42.4–52.4 Cr# and 1.9–3.5 wt.% TiO_2, while those from L4 have 40.3–46.3 Cr# and 3.1–5.8 wt.% TiO_2. Similarly, the spinels in the scoria and volcanic bomb samples of unit 3 show some differences in their chemistry: L6 spinels are characterized by 46–57.3 Cr# and 1.3–3.6 wt.% TiO_2, whereas those from L7 contain 42.5–47.2 Cr# and 2.6–4.6 wt.% TiO_2.

8.~~8~~ Discussion

The significant differences in the petrographic features, modal mineralogy, olivine textures, zoning and chemistry as well as spinel compositions observed between the discrete eruptive units (unit 1 vs. unit 2–3) indicate considerable differences in the evolution of the Fekete-hegy magmatic system prior to the phreatomagmatic and the magmatic explosive – effusive phases. Based on our results, the phreatomagmatic eruptions were preceded by a very complex pre-eruptive history. We begin by revealing the evolution of the magmatic system before the initial maar-forming eruptions, following by unraveling the history that preceded the later magmatic explosive – effusive activity.

8.1.~~8.1~~ The magmatic system that fed the initial phreatomagmatic explosive eruptive phase

8.1.1.~~8.1.1~~ Magmatic environments and their relationships recorded by olivine and spinel

The studied olivine crystals are characterized by distinct and diverse zoning patterns recorded by fast-diffusing elements such as Mg, Fe, Ni and Mn (Figs. 5, 8). These elements respond to changes in magma composition due to magma recharge or mixing, however, their compositional gradients in olivine may be extensively diffused in a few years and eliminated in a few decades (e.g., Chakraborty, 2010). This suggests that the observed zoning features in the olivines from Fekete-hegy must have been formed through relatively rapid processes. The preservation of their original zoning without any significant diffusive equilibration indicates that these olivine crystals could not have spent much time in the magmatic system prior to eruption.

Based on the diverse olivine and spinel assemblages, several distinct environments can be identified which were involved in the complex evolution of the magmatic system. Except for the type II olivines, all olivine populations show step zoning (Figs. 5 and 8), indicating the stepwise growth of the type I, III, IV and V crystals within different environments and hence the dominant role of open-system petrogenetic processes. Similar complexities and evolution were revealed through a similar olivine-focused approach by Kahl et al. (2011, 2013, 2015, 2017) in the case of Mt. Etna (Sicily). Fig. 12B displays the crystal growth stratigraphy and evolution of each olivine type in our samples. The discrete olivine portions (cores, growth zones and rims) represent the distinct environments in which they were formed and the relationships of these environments are manifested in the different zoning types. We define eight environments (A, B, C, D, E, F, G and H) that are inferred to account for the significant compositional variety of olivines. These environments can be principally distinguished in the olivine Fo vs. Cr plot (Fig. 10B). Four of these environments contributed to the formation of the diverse spinel populations (Fig. 10A). First, we introduce and characterize the individual environments and their interactions. Then, we discuss the origin and formation of these environments as well as the processes operating in the magmatic system.

Environments A, B and C: primitive basaltic magmas ('primitive magma A, B and C') in which the type I olivine cores and the type III olivine growth zones crystallized. Based on the Fo contents of these olivines ($Fo_{85–89}$) each of these magmas is characterized by 0.63–0.70 Mg# (calculated equilibrium melt Mg#), however they produced different spinel populations. Group 1 and 2 spinels were formed in primitive magmas A and B, respectively. The studied crystal clot (Fig. 9D), consisting of high-Fo olivines and group 2 spinels, also derived from primitive magma B. In the case of group 3 spinels, only the group 3a spinels originate from primitive magma C (Figs. 10A, 12B). The chemistry of spinel is primarily dependent on the composition of the melt in which it crystallizes (e.g., Irvine, 1965, 1967; Dick and Bullen, 1984; Allan et al., 1988; Arai, 1992; Roeder, 1994; Kamenetsky et al., 2001). Therefore, the significant differences observed between the Cr#s (at similar TiO_2 and Fe^{3+} contents) of the distinct spinel groups (Figs. 4C–D, 10A) reflect that they could have precipitated from separate primitive basaltic melts characterized by different Cr and Al concentrations. In addition, the presence of these three distinct primitive magmas is also supported by the variable Ni and trace element contents of the type I olivine cores and the type III olivine growth zones (Fig. 7) (see Subsection 8.1.2. for details).

Environment D: a fractionated magma which is mainly represented by the cores of the type III olivines and occasionally by type V olivine cores. There are no relatable spinel compositions for this magmatic environment. These olivine compositions ($Fo_{83–85}$) indicate Mg#s between 0.58 and 0.62 for this magma. Although similar in some aspects, this crystallization environment is distinguishable from environment E by lower Cr, P, Ca, Mn and Zn, and higher Co concentrations (Fig. 7).

Environment E: a fractionated magma that produced the type II olivine crystals, the rims of all olivine types and the group 3b spinels (the majority of the group 3 spinels). This magmatic environment was the place for the final crystallization history characterized by variable Mg# ranging between 0.50 and 0.62 based on these olivine compositions ($Fo_{78–85}$).

Environment F: an evolved magma in which the cores of the type IV olivines and the growth zones of the type V olivines crystallized. Their compositions ($Fo_{70–80}$) indicate low Mg# varying between 0.40 and 0.54 for this magmatic environment. Aside from lower Mg#, it differs from environment E in its lower-Cr and -Sc and higher-Zn olivines (Fig. 7) as well as the fact that it did not crystallize any spinels.

Environment G: lithospheric mantle peridotite wall-rock, represented by the rare high-Fo (90.6–90.9 mol%), high-NiO (0.39–0.41 wt-%) and low-CaO (0.07–0.12 wt-%) cores of type I and type V olivines. These compositions are characteristic of olivines from lithospheric mantle-derived peridotites (e.g., Boudier, 1991; Hirano et al., 2004). Thus, these olivine cores are inferred to be olivine xenocrysts, similar to occurrences in nearby volcanic centers (e.g., Jankovics et al., 2009, 2012, 2013).

Environment H: a magma distinct from the others where most of the type V olivine cores and one of the type III olivine cores were formed without spinel inclusions. It is characterized by 0.63–0.65 Mg# on the basis of these olivine compositions (85.7–86.3 mol% Fo). This Mg# range and the olivine Ca, Mn, Co, Zn and Ti contents partly overlap with those of environments A, B and C, however, these olivines show dominantly higher Ni and lower Cr, P and Sc contents (Fig. 7).

In summary, with the exception of environment G (lithospheric mantle peridotite) all identified environments are inferred to be magmatic in origin. Magmas from these environments experienced a variety of interactions with one another prior to eruption.

8.1.2.~~8.1.2~~ Origin and formation of the magmatic environments

The primitive magnesian olivines (type I olivine cores and type III olivine growth zones) show an extremely wide range of NiO contents (0.03–0.35 wt.%; Figs. 7A, 11A). Notably, these considerable NiO fluctuations can also be detected within the cores of single type I olivine crystals (even changing from 0.03 to 0.21 wt.%). Such significant Ni variations, at given high Fo contents, are commonly interpreted to be generated during partial melting of the mantle where distinct mantle lithologies are involved and melting takes place at different pressures (e.g., Sobolev et al., 2005; Herzberg, 2011). This implies that distinct batches of primitive mantle melts arrived, probably derived from different mantle source regions. Therefore, the observed large variation in the Ni concentrations of this olivine population is explained as the result of mixing between dissimilar primitive melts. To further clarify this process, we employ the three different spinel groups (group 1, 2 and 3a) which distinguish the three primitive magmas (A, B and C) (Fig. 10A). Based on the chemistry of the group 1 and 2 spinel inclusions and considering their positions within the individual olivine types, primitive magma A and primitive magma B are inferred to be two distinct, end-member primary mantle melts which could have originated from two separate mantle source regions. Similar conclusions (open-system processes and involvement of magmas derived from different mantle sources) were drawn regarding the evolution of primitive mafic magmas at long-lived polygenetic stratovolcanoes along subduction zones, using olivines and their spinel inclusions (e.g., Reubi et al., 2002). The compositions and the intra-olivine positions of our group 3a spinels indicate that primitive magma C can be considered to be a hybrid primitive basaltic magma resulting from the mixing of primitive magmas A and B.

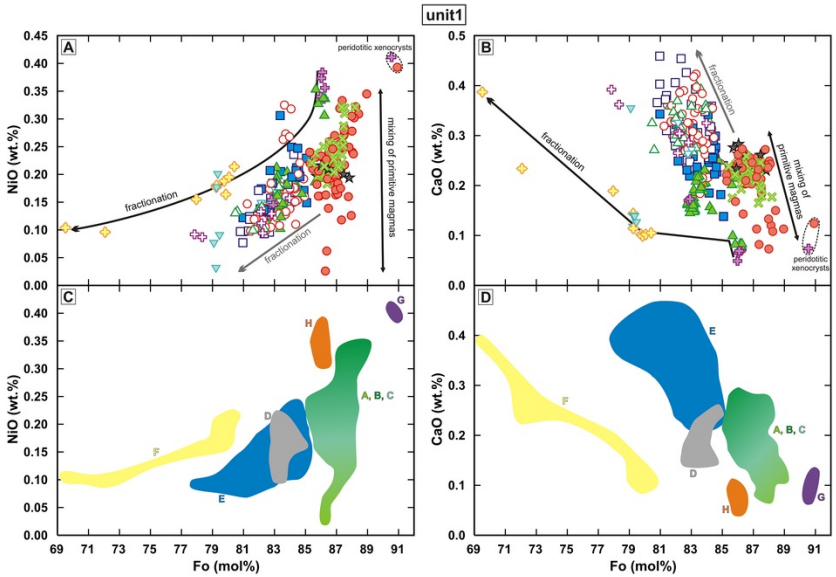

Fig. 11 Interpretation of petrogenetic processes related to the origin of the distinct environments from which the different olivine populations derived (phreatomagmatic eruptive phase – unit1).

alt-text: Fig. 11

The compositional trends shown by the group 3b spinels, i.e., the continuously increasing TiO_2 and Fe^{3+} contents (Figs. 4C–D, 10A), indicate that they were formed through fractional crystallization (e.g., Barnes and Roeder, 2001; Roeder et al., 2003). This process is also shown by the compositional variation displayed by the type II olivine crystals and all olivine rims, i.e., the continuously decreasing NiO and increasing CaO and MnO along with the continually diminishing Fo contents (e.g., Simkin and Smith, 1970; Sato, 1977) (Figs. 7A–C, 11A–B). This suggests that fractional crystallization was the dominant process in environment E. In addition, based on the compositional relationships between the type I cores + type III growth zones and the type II olivine crystals + all olivine rims, as well as between the group 3a and 3b spinels, environment E originated from the hybrid primitive magma C via fractionation (Figs. 10A, 11). This explains the already fractionated character of environment E. Accordingly, the fractionation of the mixed primitive magma C produced another magmatic environment (E) where individual olivine crystals (type II) together with all olivine rims were formed (final crystallization of all olivines).

The type III olivine cores together with sparse type V olivine cores define environment D. Although a similarly fractionated environment to E, environment D differs with regard to several elements in its olivines (Figs. 7, 10B, 11). It is important to note that aside from the smaller olivines, numerous large (1–4.5 mm) crystals occur as the cores of type III olivines (Fig. 5D). One of the studied samples contains several such large (3–5 mm) olivine crystals attached to a ~2 cm-sized clinopyroxene megacryst (colorless under the optical microscope) (Supplementary Fig. 3). These olivine grains show very similar appearances as the large type III olivine cores. They consist of numerous subgrains, mainly in their marginal parts. A number of clinopyroxene and amphibole megacrysts were found at L1, which have the same appearances and textural features as the well-studied clinopyroxene and amphibole megacrysts commonly found in other alkaline basaltic volcanics from the Bakony-Balaton Highland Volcanic Field (e.g., Embey-Isztin et al., 1990; Dobosi et al., 2003a; Jankovics et al., 2013, 2016). They generally occur together with pyroxenite (Type II) xenoliths consisting of clinopyroxene + olivine + spinel ± amphibole. Based on their major and trace element and isotopic characteristics, these megacrysts and pyroxenite xenoliths were inferred to share a common origin representing fragments of igneous cumulates crystallized from earlier alkaline basaltic magmas which did not reach the

surface. These earlier magmas stalled and accumulated in the uppermost part of the lithospheric mantle, near the crust–mantle boundary and crystallized as veins, dykes and sills characterized by compositions very similar to those representing the host alkaline basalts (e.g., Embey-Isztin et al., 1990; Dobosi et al., 2003a; Jankovics et al., 2013, 2016). Considering the co-existence of the above-mentioned large olivine grains with a clinopyroxene megacryst in our studied sample, and the appearance of the large type III olivine cores (textural features implying disaggregation; Fig. 5D), we can interpret the type III olivine cores as originating from the same igneous cumulates as the clinopyroxene and amphibole megacrysts and the pyroxenite xenoliths. Assuming a clinopyroxene + amphibole + olivine mineral assemblage for these earlier accumulated alkaline basaltic magmas, this origin can be also supported by the composition of type III olivine cores. The intermediate Fo and Ni contents of the type III olivine cores can be attributed to olivine crystallization, their low Cr concentrations could be the result of co-crystallization of clinopyroxene and their lower Ca contents may have been caused by the co-crystallization of both clinopyroxene and amphibole. Additionally, it can be assumed that during slow cooling and crystallization, these olivine crystals equilibrated, resulting in their quite homogeneous compositions observed within individual type III olivine cores. This scenario also explains why their Fo and Ni concentrations are similar to those of the olivines crystallized from environment E (because the earlier stalled alkaline basaltic magmas, represented by the cumulates, are similar in composition to the final crystallization regime, i.e., environment E).

The compositions of the type IV olivine cores and the type V olivine growth zones indicate the presence of an evolved magmatic environment (F) which according to the frequency of these olivine compositions could have played a lesser (but important) role in the magmatic system. Its origin can probably be related to environment H on the basis of the Fo vs. NiO and CaO relationships: the olivine compositions of environment F can be derived from those of environment H through fractionation (Fig. 11). Thus, the olivines of environment H occurring only as cores (of type V crystals and one type III olivine) could represent the early products of this fractionation process (as near-liquidus phases). Negative correlation between Fo and CaO contents of olivines indicates continuous crystallization with decreasing pressure, while constant or decreasing CaO can be the result of cooling at constant pressure (Stormer, 1973). This suggests that the kinked character of the Fo – CaO fractionation trend (consisting of a nearly flat and a negative part; Fig. 11B) is the result of crystallization at a nearly constant depth, followed by crystallization at continuously decreasing pressure. In general, a flat or slightly positive Fo – CaO trend dominantly at a lower Fo range can also imply the co-crystallization of olivine and clinopyroxene, as Ca is more compatible in the latter phase (Kawabata et al., 2011). The genetic relationship between environment H and F can be also proved by the trace element maps of type V olivine (Fig. 8E). This type V growth zone has the same Cr concentration as its core, suggesting that these olivine portions crystallized from petrogenetically related melts. Furthermore, the decreasing Ni and increasing Mn and Zn contents from the core to the growth zone imply that they are parts of a fractional crystallization sequence. It is noteworthy that the olivines from environment H display Ni contents much higher and Ca concentrations lower than expected for their Fo contents (Fig. 11). This suggests that this distinct magma possibly originated from a pyroxene-rich mantle source region, due to the fact that basaltic melts derived from a pyroxenitic source crystallize olivines with high Ni, and low Ca and Fo contents (e.g., Sobolev et al., 2005, 2007; Herzberg, 2011).

8.1.3.~~8.1.3~~ Evolution of the magmatic system

Here we summarize the interpretations on magmatic environments with the addition of spatial and temporal information on the pre-eruptive evolution of the sub-volcanic system. Our suggested model for the possible architecture of the magmatic system that fed the phreatomagmatic eruptive phase is shown in Fig. 12A.

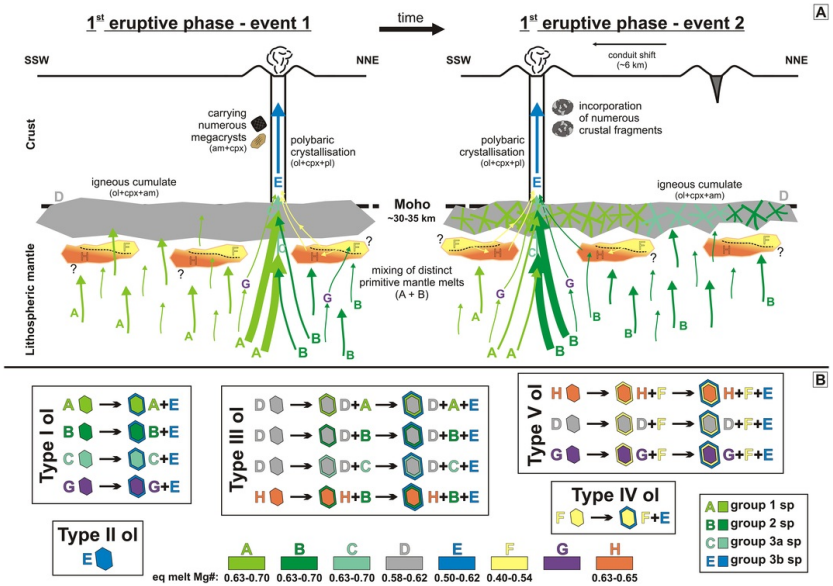

Fig. 12 (A) Possible schematic model for the evolution of the Fekete-hegy magmatic system preceding the initial phreatomagmatic eruptive phase (unit 1) (see also text for further discussion). A-H letters refer to the inferred environments. Figure is to scale vertically but is

exaggerated horizontally (approximately sevenfold). Event 1: Primitive magmas (dominantly primitive magma A) ascended and intruded into the (still stable) near-Moho igneous cumulate beneath the entire area of the present-day volcanic complex. In this stage the primitive magmas intensively interacted with the cumulate having fragmented, disaggregated and remobilized it through multiple intrusions (resulting in the abundant megacrysts in the northern samples). After the variable petrogenetic processes (mixing, replenishments, fractionation) magma batches reached the surface and produced phreatomagmatic eruptions in the northern part. Event 2: With time, the cumulate could have been more and more heated and consumed trough the multiple intrusions of the replenishing primitive magmas (primitive magma B could have become more dominant). Again, the same various processes operated as during event 1, however, it was easier for the magmas to get through the already disrupted cumulate and less material was entrained from it. The magmas incorporated a number of crustal fragments from shallower depths and erupted in the southern part. (B) Summary of the different olivine types (crystal growth stratigraphy) and spinel inclusions with the inferred distinct environments that were involved in the evolution of the magmatic system prior to the phreatomagmatic eruptive phase (unit 1).

alt-text: Fig. 12

Existence of an igneous cumulate body (environment D) is confirmed by the type III olivine cores (and rarely by type V olivine cores) and by the occurrence of clinopyroxene and amphibole megacrysts. This cumulate represents earlier accumulated alkaline basaltic magmas that did not reach the surface but stalled and crystallized near the crust-mantle boundary in the uppermost mantle, and have similar compositions as the host alkaline basalts.

The compositional variations of type I olivine cores and type III olivine growth zones as well as the occurrence of the three spinel groups indicate that two different primitive basaltic melts (A and B) probably arrived from two distinct mantle source regions and subsequently mixed with each other resulting in the formation of a hybrid primitive magma (C). This mixing could have taken place both at depth below the cumulate and within this environment as well. Each of the three primitive magmas is assumed to have intruded into environment D, as all three spinel groups occur in the growth zones of type III olivines. The fact that the type III olivine cores are overgrown by the primitive growth zones (representing environments A, B and C) implies that during replenishments these primitive magmas incorporated a number of olivine crystals from the cumulate, carrying them to shallower levels. In contrast to the type III olivine cores and growth zones, the type I olivine cores record the olivine crystallization process in primitive magmas A, B and C, without incorporating any cumulate-derived olivines. The type I cores (and the type III growth zones as well) are mostly skeletal, indicating rapid crystal growth and significant undercooling (e.g., Lofgren, 1974; Crabtree and Lange, 2011). According to the experiments of Lofgren (1974) and Hammer (2006), skeletal crystal growth can take place when a hotter magma intrudes into an environment characterized by lower temperature. This suggests that the skeletal cores of the type I olivines could have been formed during the intrusion of the hot primitive magmas (A, B and C) into the lower-temperature cumulate (environment D). Among the type I olivines, a smaller number of non-skeletal euhedral-subhedral cores occur, implying that the intruding primitive magmas could have already carried their high-Fo olivines (having crystallized in greater depths) to this environment. Based on these processes the ascending primitive basaltic magmas both intersected and remobilized the igneous cumulate (environment D).

Fractionation of the hybrid primitive magma C, producing the magmatic environment E, could have occurred after the intersection and remobilization of the cumulate. This fractionation process is directly indicated by sparse type I olivine crystals where the core-to-rim compositional change is continuous rather than abrupt. However, the step zoning that dominantly characterizes the type I olivines implies that these two environments (C and E) must have also co-existed in the magmatic system at some point in time. This allowed the arrival of primitive magma C carrying high-Fo olivines (type I cores) into environment E where they were overgrown by lower-Fo olivine (type I rims). This magmatic environment (E) was the final place for olivine crystallization where the rims of each olivine types were formed through polybaric crystallization.

The genetically related environments F and H are assumed to mutually represent a distinct magmatic body, located below the igneous cumulate (environment D), where F and H could have been separated from one another. Similar to the case of environments C and E, these two environments should also have existed simultaneously, based on the step zoning observed in type V olivines, with cores originating from environment H. These type V olivines record the process when the evolved magma (F) could have incorporated olivines from environment H and brought them further into environment E. One of the type III olivine cores also derives from environment H and is surrounded by a primitive growth zone containing both group 2 and group 3a spinels (Fig. 9C). This suggests that primitive magma B could have incorporated olivine crystal(s) from environment H during its ascent and carried it/them into the cumulate body (environment D) where a possible interaction with primitive magma C might have occurred based on the co-existence of group 2 and 3 spinels.

The presence of sparse lithospheric mantle-derived olivine xenocrysts, occurring as rare cores of type I and type V olivines, implies that these foreign crystals were entrained into the ascending primitive magmas from the peridotite wall rock (environment G). These xenocrysts were transported directly into environment E (in the case of type I olivine) or first into environment F (in the case of type V olivine) and then transported further by the evolved magma (F).

In summary, the evolution of the magmatic system that fed the initial phreatomagmatic phase is characterized by a remarkable complexity involving a number of distinct environments with multiple magma pockets and various interactions between them. Magma stalling, accumulation, storage and fractionation are considered as closed-system processes, ~~whilst~~ while open-system processes are represented by mixing, replenishments, cumulate remobilization and incorporation of foreign fragments and crystals from the wall rocks.

Various olivine populations were reported by Ruprecht and Plank (2013) and Oeser et al. (2018) from the 1963–65 eruption products of Irazú, one of the most voluminous active volcanoes in Costa Rica. In its hybrid magmas (resulted from the mixing of basaltic and dacitic end-members; Alvarado et al., 2006) three different olivine types were distinguished, showing characteristics very similar to those of our type I, II and III olivines. These Irazú olivines were inferred to have experienced very similar processes during their formation; mixing of high-Fo mantle melts, remobilization of an igneous cumulate by the ascending primitive melts, a common late-stage crystallization history for all olivine types (Ruprecht and Plank, 2013; Oeser et al.,

2018). It is notable that in our case, the magmatic system can be characterized by such a complex evolution and even more olivine types are present, indicating the involvement of more environments and processes. This emphasizes our important conclusion that small-volume basaltic monogenetic systems (after Németh and Kereszturi, 2015; Smith and Németh, 2017) tend to show very complex pre-eruptive histories, a well-known aspect of plumbing systems of voluminous polygenetic arc volcanoes.

8.2.~~8.2~~ The magmatic system that fed the magmatic explosive – effusive eruptive phase

The studied samples of unit 2 and 3 show considerable differences compared to those of unit 1. They are characterized by a simple petrographic appearance, the olivine crystals are unvaried and only display progressive normal zoning (Fig. 6). The core-to-rim compositional variations of these olivines, i.e., the continually decreasing NiO and increasing CaO alongside continuously diminishing Fo contents (Fig. 4A–B) indicate a normal olivine fractionation trend (e.g., Simkin and Smith, 1970). The olivine-hosted spinel inclusions have a small range in Cr# (40.3–57.3) and show increasing TiO_2 and Fe^{3+} contents (Fig. 4C–D), implying that they were formed through fractional crystallization (e.g., Barnes and Roeder, 2001). Their compositions are very similar to those of the group 2 spinels in the unit 1 samples, suggesting that these spinels may have crystallized from magmas very similar to primitive magma B of unit 1.

According to the petrographic features, the main crystallizing phase was olivine accompanied by spinel. In these unit 2–3 samples, we did not observe any signs of open-system petrogenetic processes, nor the complexities discovered in the unit 1 samples. This suggests that only simple, closed-system fractional crystallization of olivine + spinel could have occurred in the case of the magmas that fed the later magmatic explosive – effusive eruptions.

Based on the whole-rock compositions of the lava, scoria and bomb samples (Fig. 3) these magmas are characterized by different degrees of fractionation. The most primitive magma erupted in the northern part (L2), the southern lava (L4) is less primitive and the scoria cones (L6 and L7) were fed by the most evolved magmas. Consequently, during the magmatic explosive – effusive phase, primitive magma batches rarely reached the surface. Most of them likely stalled near the Moho, resulting in the formation of a magma accumulation zone where they experienced a simple evolution through fractional crystallization.

8.3.~~8.3~~ Implications for the spatial and temporal evolution of the volcanic complex

A few differences were observed between the northern and southern phreatomagmatic eruptive products, yielding implications for the spatial and temporal evolution of the volcanic complex (Fig. 12A). Megacrysts of amphiboles and clinopyroxenes occur only in the northern area, with the amount of large type III olivines being much higher. This implies that the primitive magmas incorporated a large number of fragments and crystals from the near-Moho cumulate in the northern part of the magmatic system, indicating that, in this area, the cumulate and its remobilization could have played a much more significant role during the evolution of the magmatic system.

Juvenile basalt fragments from L5 contain a large amount of crustal siliciclastic xenoliths showing textural characteristics resulted from partial melting by the host basaltic magma. This implies that ascending magmas in the southern part of the system also effectively interacted with the wall rocks at upper and/or mid-crustal level(s) after the incorporation of numerous fragments from lithospheric mantle peridotites.

Group 1 spinels are more frequent in the northern part, while group 2 spinels are only present in the southern part. This suggests that primitive magma A could have played a more dominant role in the northern part, ~~whilst~~ while primitive magma B could have been the predominant primitive mantle melt in the southern part of the magmatic system. However, both primitive melts must have been present in the entire system to enable their mixing and the subsequent formation of environment E, through the fractionation of the hybrid primitive magma C. In addition, the simple olivines from unit 2–3 only host spinel inclusions similar in composition to the group 2 spinels from unit 1. This could illustrate that after the initial phreatomagmatic eruption phase, primitive magmas with very similar compositions to primitive magma B could have occupied the magmatic system, experienced various degrees of fractionation and fed the later eruptive phase.

Similar or even more pronounced petrographic differences were shown by Re et al. (2017) within a much smaller (~2 km^2) monogenetic complex, where they suggested that at least two physically separate (although near to one another) magma batches, originating from a shared source at depth, erupted at different times.

Our results provide important new data to complete our understanding of the Fekete-hegy volcanic complex. Auer et al. (2007) revealed the shallow subsurface processes and the main external forces governed the magma fragmentation, pyroclast transportation and deposition. Here, we targeted the deeper processes and unraveled the evolution of the sub-volcanic magmatic system through its entire lifespan. Together, these two works yield a source-to-surface petrogenetic-volcanological model for the volcanic complex.

According to our petrogenetic study, we propose the following model for the magmatic and volcanic history for the Fekete-hegy volcanic complex (Fig. 12). Primitive magmas (dominantly primitive magma A) ascended and intruded into the (still stable) near-Moho igneous cumulate beneath the entire area of the present-day volcanic complex. In this stage, the primitive magmas intensively interacted with the cumulate having fragmented, disaggregated and remobilized it through multiple intrusions. Following the variable petrogenetic processes (mixing, replenishments, fractionation), magma batches reached the surface and produced phreatomagmatic eruptions in the northern part. Over time, the cumulate could have undergone progressive heating and consumption through multiple intrusions of the replenishing primitive magmas (primitive magma B could have become more dominant). Again, the same various processes operated as before, however, it became easier for the magmas to get through the already disrupted cumulate, and less material was entrained from it. The magmas incorporated a number of crustal fragments from shallower

depths and erupted in the southern part (Fig. 12A). Alternatively, the cumulate may have been thicker in the northern part, and therefore more difficult for the magmas to intersect, subsequently carrying abundant cumulate-derived crystals. Later, after phreatomagmatic activity concluded, the new eruptive phase (fed from the already simple, i.e., evacuated magmatic system), produced lava flows which covered the whole area of the volcanic complex, as well as magmatic explosive eruptions building scoria cones. In spite of the lack of information concerning the exact time interval between the initial phreatomagmatic eruptive phase and the subsequent magmatic explosive – effusive phase, the significant change in the architecture and evolution of the magmatic system after the maar-forming eruptions suggests a considerable time gap between the two phases.

9.9 Conclusions

This study demonstrates that the combination of detailed textural investigations with SEM, in situ EMPA analyses, high-resolution LA-ICP-MS trace element crystal mapping and single spot measurements on diversely zoned olivines, coupled with the detailed analysis of the chemistry and occurrence of their spinel inclusions, serves as a powerful tool to unravel the evolution of basaltic systems.

Both complex and simple petrographic types of small-volume basalts are present within the studied monogenetic volcanic complex, represented by unit 1 and unit 2–3, respectively. Our results indicate a significant change during the evolution of the sub-volcanic magmatic system feeding the Fekete-hegy volcanic complex; the initial phreatomagmatic eruptive phase (unit 1) was preceded by an unexpectedly complex and well-preserved history, while the pre-eruptive processes of the later magmatic explosive – effusive phase (unit 2–3) were much simpler.

With regard to unit 1, detailed analysis of the crystal growth stratigraphy of the various olivine types suggests the involvement of eight distinct environments, with diverse origins and interactions. Four of these environments are inferred to account for the significant compositional variation of the olivine-hosted spinel inclusions. A complex set of open- and closed-system petrogenetic processes operated during the evolution of the magmatic system: magma stalling, accumulation, storage, fractionation, mixing, replenishments, cumulate remobilization, incorporation of foreign fragments and crystals from the wall rocks. All these diverse environments and processes resulted in the mixed character of the erupted magmas.

In contrast, the uniform petrological features and the small variations displayed by the olivine and spinel crystals from unit 2–3 indicate that this later eruptive phase was preceded by a considerable change in the magmatic system; it experienced a simple evolution through olivine + spinel fractional crystallization without any of the complexities seen during the initial phase.

Following the findings of our previous works in the western Pannonian Basin (Jankovics et al., 2012, 2013, 2015, 2016), the present study further emphasizes the importance of high-resolution mineral-scale textural and chemical investigations to discover the complexity of the magmatic systems feeding monogenetic basaltic volcanoes. This method enables a direct and more detailed insight into the architecture and evolution of these systems, which is essential to complement the whole-rock geochemical analyses. This is also markedly indicated by the significant difference between the range of Mg#s shown by the whole-rock data (0.66–0.72) and the equilibrium liquid compositions (0.40–0.70) calculated from the Fo contents of the diverse olivine crystals (unit 1).

It is important to highlight that the petrogenesis of a single magma batch – usually considered as representing a given eruptive unit – can be as complex as involving multiple small magma pockets from various magmatic environments, as well as diverse closed- and open-system processes, which together finally result in the bulk-rock (erupted magma) composition. These results provide fundamental advances in our view about the evolution of sub-volcanic magmatic systems through the entire lifespan of compound monogenetic volcanic complexes.

Supplementary data to this article can be found online at https://doi.org/10.1016/j.jvolgeores.2018.11.027.

Uncited references

~~Csontos, 1995~~

~~Dobosi, 1989~~

~~Embey-Isztin, 1976~~

~~Harangi et al., 1994~~

~~Németh, 2010~~

Acknowledgements

We are grateful to Lucy E. McGee and Marco Brenna for their constructive reviews, valuable suggestions and comments which helped to improve the first version of the manuscript. In this research, M. Éva

Jankovics was partly supported by the European Union and the State of Hungary, co-financed by the European Social Fund in the framework of TÁMOP 4.2.4. A/2-11-1-2012-0001 'National Excellence Program'. The TÉT_10-1-2011-0694 project (Hungarian-Austrian Cooperation) as well as the Collegium Hungaricum scholarship ~~(in Vienna)~~ of the Balassi Institute provided partial financial support. Zsolt Bendő and Franz Kiraly are acknowledged for their help during the SEM and EMPA analyses. Cooperation of Károly Németh and Tamás Sági was supported by the Erasmus+ programme (2017-2019 Erasmus+ ICM, ELTE-Massey University) of the European Union.

References

Allan J.F., Sack R.O. and Batiza R., Cr-rich spinels as petrogenetic indicators; MORB-type lavas from the Lamont seamount chain, eastern Pacific, *Am. Mineral.* **73** (7–8), 1988, 741–753.

Alvarado G.E., Carr M.J., Turrin B.D., Swisher I.I.I.C.C., Schmincke H.-U. and Hudnut K.W., Recent volcanic history of Irazú volcano, Costa Rica: Alternation and mixing of two magma batches, and pervasive mixing, In: Rose W.I., Bluth G.J.S., Carr M.J., Ewert J.W., Patino L.C. and Vallance J.W., (Eds.), *Volcanic Hazards in Central America,* 2006, Geological Society of America, 259–276.

Arai S., Chemistry of chromian spinel in volcanic rocks as a potential guide to magma chemistry, ~~*Mineralogical Magazine*~~*Mineral. Mag.* **56**, 1992, 173–184.

Astbury R.L., Petrelli M., Ubide T., Stock M.J., Arienzo I., D'Antonio M. and Perugini D., Tracking plumbing system dynamics at the Campi Flegrei caldera, Italy: High-resolution trace element mapping of the Astroni crystal cargo, *Lithos* **318–319**, 2018, 464–477.

Auer A., Martin U. and Németh K., The Fekete-hegy (Balaton Highland Hungary) "soft-substrate" and "hard-substrate" maar volcanoes in an aligned volcanic complex – Implications for vent geometry, subsurface stratigraphy and the palaeoenvironmental setting, ~~*Journal of Volcanology and Geothermal Research*~~*J. Volcanol. Geotherm. Res.* **159** (1–3), 2007, 225–245.

Bada G. and Horváth F., On the structure and tectonic of the Pannonian Basin and surrounding orogens, ~~*Acta Geologica Hungarica*~~*Acta Geol. Hung.* **44** (2–3), 2001, 301–327.

Bada G., Horváth F., Gerner P. and Fejes I., Review of the present-day geodynamics of the Pannonian basin: progress and problems, ~~*Journal of Geodynamics*~~*J. Geodyn.* **27** (4–5), 1999, 501–527.

Balogh K., Árva-Sós E., Pécskay Z. and Ravasz-Baranyai L., K/Ar dating of post-Sarmatian alkali basaltic rocks in Hungary, *Acta Mineral. Petrogr. Szeged.* **28**, 1986, 75–93.

Barnes S.J. and Roeder P.L., The Range of Spinel Compositions in Terrestrial Mafic and Ultramafic Rocks, ~~*Journal of Petrology*~~*J. Petrol.* **42** (12), 2001, 2279–2302.

Blundy J. and Cashman K., Petrologic Reconstruction of Magmatic System Variables and Processes, ~~*Reviews in Mineralogy and Geochemistry*~~*Rev. Mineral. Geochem.* **69** (1), 2008, 179–239.

Boudier F., Olivine xenocrysts in picritic magmas, ~~*Contributions to Mineralogy and Petrology*~~*Contrib. Mineral. Petrol.* **109** (1), 1991, 114–123.

Boyce J., Nicholls I., Keays R. and Hayman P., Variation in parental magmas of Mt Rouse, a complex polymagmatic monogenetic volcano in the basaltic intraplate Newer Volcanics Province, southeast Australia, *Contrib. Mineral. Petrol.* **169** (2), 2015, 1–21.

Brenna M., Cronin S.J., Smith I.E.M., Sohn Y.K. and Németh K., Mechanisms driving polymagmatic activity at a monogenetic volcano, Udo, Jeju Island, South Korea, *Contrib. Mineral. Petrol.* **160** (6), 2010, 931–950.

Brenna M., Cronin S.J., Németh K., Smith I.E.M. and Sohn Y.K., The influence of magma plumbing complexity on monogenetic eruptions, Jeju Island, Korea, *Terra Nova* 2011, 1–6.

Brenna M., Cronin S.J., Smith I.E., Tollan P.M., Scott J.M., Prior D.J., Bambery K. and Ukstins I.A., Olivine xenocryst diffusion reveals rapid monogenetic basaltic magma ascent following complex storage at Pupuke Maar, Auckland Volcanic Field, New Zealand, ~~*Earth and Planetary Science Letters*~~*Earth Planet. Sci. Lett.* **499**, 2018, 13–22.

Chakraborty S., Diffusion coefficients in olivine, wadsleyite and Ringwoodite, *Rev. Mineral. Geochem.* **72** (1), 2010, 603–639.

Clynne M.A. and Borg L.E., Olivine and chromian spinel in primitive calc-alkaline and tholeiitic lavas from the southernmost Cascade Range, California; a reflection of relative fertility of the source, ~~*The Canadian Mineralogist*~~*Can. Mineral.* **35** (2), 1997, 453–472.

Crabtree S.M. and Lange R.A., Complex phenocryst textures and zoning patterns in andesites and dacites: evidence of degassing-induced crystallization?, ~~*Journal of Petrology*~~*J. Petrol.* **52**, 2011, 3–38.

Csontos L., Tertiary tectonic evolution of the intra-carpathian area: ~~A~~a review, ~~*Acta Vulcanologica*~~*Acta Vulcanol.* **7**, 1995, 1–13.

Csontos L., Nagymarosy A., Horváth F. and Kovác M., Tertiary evolution of the Intra-Carpathian area: Aa model, *Tectonophysics* **208** (1–3), 1992, 221–241.

Davidson J.P., Morgan D.J., Charlier B.L.A., Harlou R. and Hora J.M., Microsampling and Isotopic Analysis of Igneous Rocks: Implications for the Study of Magmatic Systems, *Annual Review of Earth and Planetary SciencesAnnu. Rev Earth Planet. Sci.* **35** (1), 2007, 273–311.

de Maisonneuve C.B., Costa F., Huber C., Vonlanthen P., Bachmann O. and Dungan M.A., How do olivines record magmatic events? Insights from major and trace element zoning, *Contributions to Mineralogy and PetrologyContrib. Mineral. Petrol.* **171** (6), 2016, 56.

Dégi J., Abart R., Török K., Rhede D. and Petrishcheva E., Evidence for xenolith-host basalt interaction from chemical patterns in Fe-Ti-oxides from mafic granulite xenoliths of the Bakony-Balaton Volcanic field (W-Hungary), *Mineralogy and PetrologyMineral. Petrol.* **95** (3), 2009, 219–234.

Dick H.J.B. and Bullen T., Chromian spinel as a petrogenetic indicator in abyssal and alpine-type peridotites and spatially associated lavas, *Contributions to Mineralogy and PetrologyContrib. Mineral. Petrol.* **86** (1), 1984, 54–76.

Dobosi G., Clinopyroxene zoning patterns in the young alkali basalts of Hungary and their petrogenetic significance, *Contributions to Mineralogy and PetrologyContrib. Mineral. Petrol.* **101**, 1989, 112–121.

Dobosi G., Downes H., Embey-Isztin A. and Jenner G.A., Origin of megacrysts and pyroxenite xenoliths from the Pliocene alkali basalts of the Pannonian Basin (Hungary), *Neues Jb. Mineral. Abh.* **178** (3), 2003a, 217–237.

Dobosi G., Kempton P.D., Downes H., Embey-Isztin A., Thirlwall M. and Greenwood P., Lower crustal granulite xenoliths from the Pannonian Basin, Hungary, Ppart 2: Sr–Nd–Pb–Hf and O isotope evidence for formation of continental lower crust by tectonic emplacement of oceanic crust, *Contributions to Mineralogy and PetrologyContrib. Mineral. Petrol.* **144** (6), 2003b, 671–683.

Downes H. and Vaselli O., The lithospheric mantle beneath the Carpathian-Pannonian Region: a review of trace element and isotopic evidence from ultramafic xenoliths, *Acta VulcanologicaActa Vulcanol.* **7**, 1995, 219–229.

Downes H., Embey-Isztin A. and Thirlwall M.F., Petrology and geochemistry of spinel peridotite xenoliths from the western Pannonian Basin (Hungary): evidence for an association between enrichment and texture in the upper mantle, *Contributions to Mineralogy and PetrologyContrib. Mineral. Petrol.* **109** (3), 1992, 340–354.

Embey-Isztin A., Amphibolite/lherzolite composite xenolith from Szigliget, north of the lLake Balaton, Hungary, *Earth and Planetary Science LettersEarth Planet. Sci. Lett.* **31** (2), 1976, 297–304.

Embey-Isztin A. and Dobosi G., Mantle source characteristics for Miocene-Pleistocene alkali basalts, Carpathian-Pannonian Region: Aa review of trace elements and isotopic composition, *Acta VulcanologicaActa Vulcanol.* **7**, 1995, 155–166.

Embey-Isztin A., Scharbert H.G., Dietrich H. and Poultidis H., Petrology and Geochemistry of Peridotite Xenoliths in Alkali Basalts from the Transdanubian Volcanic Region, West Hungary, *J. Petrol.* **30** (1), 1989, 79–105.

Embey-Isztin A., Scharbert H.G., Dietrich H. and Poultidis H., Mafic granulites and clinopyroxenite xenoliths from the Transdanubian Volcanic Region (Hungary): implications for the deep structure of the Pannonian Basin, *Mineralogical MagazineMineral. Mag.* **54**, 1990, 463–483.

Embey-Isztin A., Downes H., James D.E., Upton B.G.J., Dobosi G., Ingram G.A., Harmon R.S. and Scharbert H.G., The petrogenesis of Pliocene alkaline volcanic rocks from the Pannonian Basin, Eastern Central Europe, *J. Petrol.* **34**, 1993, 317–343.

Embey-Isztin A., Downes H. and Dobosi G., Geochemical characterization of the Pannonian Basin mantle lithosphere and asthenosphere: an overview, *Acta Geologica HungaricaActa Geol. Hung.* **44** (2–3), 2001, 259–280.

Embey-Isztin A., Downes H., Kempton P.D., Dobosi G. and Thirlwall M., Lower crustal granulite xenoliths from the Pannonian Basin, Hungary. Part 1: mineral chemistry, thermobarometry and petrology, *Contributions to Mineralogy and PetrologyContrib. Mineral. Petrol.* **144**, 2003, 652–670.

Erlund E.J., Cashman K.V., Wallace P.J., Pioli L., Rosi M., Johnson E. and Granados H.D., Compositional evolution of magma from Parícutin Volcano, Mexico: Tthe tephra record, *Journal of Volcanology and Geothermal ResearchJ. Volcanol. Geotherm. Res.* **197** (1–4), 2010, 167–187.

Fodor L., Csontos L., Bada G., Benkovics L. and Györfi I., Tertiary tectonic evolution of the Carpatho-Pannonian region: A new synthesis of palaeostress data, In: Durand B., Jolivet L., F. H. and Séranne M., (Eds.), *The Mediterranean Basins: Tertiary Extension within the Alpine Orogen, Special Publications* 1999, Geological Society; London, 295–334.

Gao S., Xiaomin L., Yuan H., Hattendorf B., Günther D., Chen L. and Hu S., Determination of forty two major and trace elements in USGS and NIST SRM glasses by laser ablation-inductively coupled plasma-mass spectrometry, ~~*Geostandards Newsletter*~~*Geostand. Newslett.* **26**, 2002, 181–196.

Gernon T.M., Upton B.G.J., Ugra R., Yücel C., Taylor R.N. and Elliott H., Complex subvolcanic magma plumbing system of an alkali basaltic maar-diatreme volcano (Elie Ness, Fife, Scotland), *Lithos* **264**, 2016, 70–85.

Ginibre C., Wörner G. and Kronz A., Crystal Zoning as an Archive for Magma Evolution, *Elements* **3** (4), 2007, 261–266.

Hammer J.E., Influence of fO_2 and cooling rate on the kinetics and energetics of Fe-rich basalt crystallization, ~~*Earth and Planetary Science Letters*~~*Earth Planet. Sci. Lett.* **248**, 2006, 618–637.

Harangi S. and Lenkey L., Genesis of the Neogene to Quaternary volcanism in the Carpathian-Pannonian region: Role of subduction, extension, and mantle plume, *Geol. Soc. Am. Spec. Pap.* **418**, 2007, 67–92.

Harangi S., VaseIli O., Kovács R., Tonarini S., Coradossi N. and Ferraro D., Volcanological and magmatological studies on the Neogene basaltic volcanoes of the Southern LittIe Hungarian Plain, Pannonian Basin (Western Hungary), *Mineral. Petrogr. Acta* **37**, 1994, 183–197.

Harangi S., Ságí T., Seghedi I. and Ntaflos T., Origin of basaltic magmas of Perşani volcanic field, Romania: ~~A~~a combined whole rock and mineral scale investigation, *Lithos* **180–181**, 2013, 43–57.

Harangi S., Jankovics M.É., Ságí T., Kiss B., Lukács R. and Soós I., Origin and geodynamic relationships of the Late Miocene to Quaternary alkaline basalt volcanism in the Pannonian basin, eastern-c~~C~~entral Europe, *Int. J. Earth Sci. (Geol. Rundsch)* 2015, 1–26.

Herzberg C., Basalts as temperature probes of Earth's mantle, *Geology* **39** (12), 2011, 1179–1180.

Hidas K., Falus G., Szabó C., Szabó P.J., Kovács I. and Földes T., Geodynamic implications of flattened tabular equigranular textured peridotites from the Bakony-Balaton Highland Volcanic Field (Western Hungary), ~~*Journal o Geodynamics*~~*J. Geodyn.* **43** (4~~-~~5), 2007, 484–503.

Hirano N., Yamamoto J., Kagi H. and Ishii T., Young, olivine xenocryst-bearing alkali-basalt from the oceanward slope of the Japan Trench, ~~*Contributions to Mineralogy and Petrology*~~*Contrib. Mineral. Petrol.* **148** (1), 2004, 47–54.

Horváth F., Phases of compression during the evolution of the Pannonian Basin and its bearing on hydrocarbon exploration, ~~*Marine and Petroleum Geology*~~*Mar. Pet. Geol.* **12** (8), 1995, 837–844.

Horváth F. and Cloetingh S., Stress-induced late-stage subsidence anomalies in the Pannonian Basin, *Tectonophysics* **266** (1~~-~~4), 1996, 287–300.

Horváth F., Bada G., Szafián P., Tari G., Ádám A. and Cloetingh S., Formation and deformation of the Pannonian basin, In: Gee D.G. and Stephenson R.A., (Eds.), *European Lithosphere Dynamics,* 2006, Geol Soc Lond Mem, 191–207.

Horváth F., Musitz B., Balázs A., Végh A., Uhrin A., Nádor A., Koroknai B., Pap N., Tóth T. and Wórum G., Evolution of the Pannonian basin and its geothermal resources, *Geothermics* **53**, 2015, 328–352.

Irvine T.N., Chromian Spinel as a Petrogenetic Indicator: ~~P~~part 1. Theory, *Can. J. Earth Sci.* **2** (6), 1965, 648–672.

Irvine T.N., Chromian spinel as a petrogenetic indicator: ~~P~~part 2. Petrologic applications, *Can. J. Earth Sci.* **4** (1), 1967, 71–103.

Jankovics É., Harangi S. and Ntaflos T., A mineral-scale investigation on the origin of the 2.6 Ma Füzes-tó basalt, Bakony-Balaton Highland Volcanic Field (Pannonian Basin, Hungary), *Central European Geol.* **52** (2), 2009, 97–124.

Jankovics M.É., Harangi S., Kiss B. and Ntaflos T., Open-system evolution of the Füzes-tó alkaline basaltic magma, western Pannonian Basin: Constraints from mineral textures and compositions, *Lithos* **140-141**, 2012, 25–37.

Jankovics M.É., Dobosi G., Embey-Isztin A., Kiss B., Ságí T., Harangi S. and Ntaflos T., Origin and ascent history of unusually crystal-rich alkaline basaltic magmas from the western Pannonian Basin, ~~*Bull Volcanol.*~~*Bull. Volcanol.* **75** (9), 2013, 1–23.

Jankovics M.É., Harangi S., Németh K., Kiss B. and Ntaflos T., A complex magmatic system beneath the Kissomlyó monogenetic volcano (western Pannonian Basin): evidence from mineral textures, zoning and chemistry, *J. Volcanol. Geotherm. Res.* **301**, 2015, 38–55.

Jankovics M.É., Taracsák Z., Dobosi G., Embey-Isztin A., Batki A., Harangi S. and Hauzenberger C.A., Clinopyroxene with diverse origins in alkaline basalts from the western Pannonian Basin: Implications from trace element characteristics, *Lithos* **262**, 2016, 120–134.

Jochum K.P., Willbold M., Raczek I., Stoll B. and Herwig K., Chemical characterisation of the USGS reference glasses GSA-1G, GSC1G, GSD-1G, GSE-1G, BCR-2G, BHVO-2G and BIR-1G using EPMA, ID-TIMS. ID-ICP-MS and LA-ICP-MS, ~~*Geostandards and Geoanalytical Research*~~*Geostand. Geoanal. Res.* **29** (3), 2005, 285–302.

Jugovics L., The Transdanubian basalt and basaltic tuff fields (in Hungarian), In: *Yearly Report of the Hungarian Geological Institute About the Year,* **1967**, 1968, 75–82.

Jugovics L., The chemical character of the Hungarian basalts (in Hungarian), In: *Yearly Report of the Hungarian Geological Institute about the year,* **1974**, 1976, 431–470.

Kahl M., Chakraborty S., Costa F. and Pompilio M., Dynamic plumbing system beneath volcanoes revealed by kinetic modeling, and the connection to monitoring data: ~~A~~an example from Mt. Etna, *Earth Planet. Sci. Lett.* **308** (1–2), 2011, 11–22.

Kahl M., Chakraborty S., Costa F., Pompilio M., Liuzzo M. and Viccaro M., Compositionally zoned crystals and real-time degassing data reveal changes in magma transfer dynamics during the 2006 summit eruptive episodes of Mt. Etna, *Bull. Volcanol.* **75** (692), 2013.

Kahl M., Chakraborty S., Pompilio M. and Costa F., Constraints on the Nature and Evolution of the Magma Plumbing System of Mt. Etna Volcano (1991–2008) from a ~~C~~combined Thermodynamic and Kinetic Modelling of the Compositional Record of Minerals, ~~*Journal of Petrology*~~*J. Petrol.* **56** (10), 2015, 2025–2068.

Kahl M., Viccaro M., Ubide T., Morgan D.J. and Dingwell D.B., A branched magma feeder system during the 1669 eruption of Mt Etna: ~~E~~evidence from a time-integrated study of zoned olivine phenocryst populations, ~~*Journal of Petrology*~~*J. Petrol.* **58** (3), 2017, 443–472.

Kamenetsky V.S., Crawford A.J. and Meffre S., Factors controlling chemistry of magmatic spinel: an empirical study of associated olivine, Cr-spinel and melt inclusions from primitive rocks, ~~*Journal of Petrology*~~*J. Petrol.* **42** (4), 2001, 655–671.

Kawabata H., Hanyu T., Chang Q., Kimura J.-I., Nichols A.R.L. and Tatsumi Y., The petrology and geochemistry of St. Helena alkali basalts: evaluation of the oceanic crust-recycling model for HIMU OIB, ~~*Journal of Petrology*~~*J. Petrol.* **52** (4), 2011, 791–838.

Kempton P.D., Downes H. and Embey-Isztin A., Mafic granulite xenoliths in neogene alkali basalts from the Western Pannonian basin: insights into the lower Crust of a collapsed orogen, ~~*Journal of Petrology*~~*J. Petrol.* **38** (7), 1997, 941–970.

Kereszturi G., Csillag G., Németh K., Sebe K., Balogh K. and Jáger V., Volcanic architecture, eruption mechanism and landform evolution of a Pliocene intracontinental basaltic polycyclic monogenetic volcano from the Bakony-Balaton Highland Volcanic Field, Hungary, *Central European J. Geosci.* **2** (3), 2010, 362–384.

Kereszturi G., Németh K., Csillag G., Balogh K. and Kovács J., The role of external environmental factors in changing eruption styles of monogenetic volcanoes in a Mio/Pleistocene continental volcanic field in western Hungary, ~~*Journal of Volcanology and Geothermal Research*~~*J. Volcanol. Geotherm. Res.* **201** (1), 2011, 227–240.

Kovács I.J., Falus G., Stuart G., Hidas K., Szabó C., Flower M.F.J., Hegedűs E., Posgay K. and Zilahi-Sebess L., Seismic anisotropy and deformation patterns in upper mantle xenoliths from the central Carpathian–Pannonian region: Asthenospheric flow as a driving force for Cenozoic extension and extrusion?, *Tectonophysics* **514-517**, 2012, 168–179.

Landi P., Corsaro R.A., Francalanci L., Civetta L., Miraglia L., Pompilio M. and Tesoro R., Magma dynamics during the 2007 Stromboli eruption (Aeolian Islands, Italy): Mineralogical, geochemical and isotopic data, *J. Volcanol. Geotherm. Res.* **182**, 2009, 255–268.

Le Bas M.J., Maitre R.W.L., Streckeisen A., Zanettin B. and Rocks I.S.o.t.S.o.I., A chemical classification of volcanic rocks ~~B~~based on the total alkali-silica diagram, ~~*Journal of Petrology*~~*J. Petrol.* **27** (3), 1986, 745–750.

Lenkey L., Dövényi P., Horváth F. and Cloetingh S., Geothermics of the Pannonian Basin and its Bearing on the Neotectonics, *European Geophysical Union Stephan Mueller Special Publications, Series* **3**, 2002, 29–40.

Lofgren G., An experimental study of plagioclase crystal morphology: isothermal crystallization, ~~*American Journal of Science*~~*Am. J. Sci.* **274**, 1974, 243–273.

Longpré M.-A., Klügel A., Diehl A. and Stix J., Mixing in mantle magma reservoirs prior to and during the 2011–2012 eruption at El Hierro, Canary Islands, *Geology* **42** (4), 2014, 315–318.

Martí J., Castro A., Rodríguez C., Costa F., Carrasquilla S., Pedreira R. and Bolos X., Correlation of Magma Evolution and Geophysical Mmonitoring during the 2011–2012 El Hierro (Canary Islands) Submarine Eruption, *Journal of Petrology J. Petrol.* **54** (7), 2013, 1349–1373.

Martin U. and Németh K., Mio/Pliocene Phreatomagmatic Volcanism in the Western Pannonian Basin, 2004, Geological Institute of Hungary; Budapest.

Martin U., Németh K., Auer A. and Breitkreuz C., Mio-Pliocene Phreatomagmatic Volcanism in a Fluvio-Lacustrine Basin in Western Hungary, *GeolinesAndean Geol.* **15**, 2003, 84–90.

McGee L.E. and Smith I.E.M., Interpreting chemical compositions of small scale basaltic systems: Aa review, *Journal of Volcanology and Geothermal ResearchJ. Volcanol. Geotherm. Res.* **325**, 2016, 45–60.

McGee L.E., Millet M.-A., Smith I.E.M., Németh K. and Lindsay J.M., The inception and progression of melting in a monogenetic eruption: Motukorea Volcano, the Auckland Volcanic Field, New Zealand, *Lithos* **155** (0), 2012, 360–374.

Nakamura N., Determination of REE, Ba, Fe, Mg, Na and K in carbonaceous and ordinary chondrites, *Geochimica et Cosmochimica ActaGeochim. Cosmochim. Acta* **38** (5), 1974, 757–775.

Németh K., Monogenetic volcanic fields: Origin, sedimentary record, and relationship with polygenetic volcanism, *Geol. Soc. Am. Spec. Pap.* **470**, 2010, 43–66.

Németh K. and Kereszturi G., Monogenetic volcanism: personal views and discussion, *International Journal of Earth SciencesInt. J. Earth Sci.* **104**, 2015, 2131–2146.

Németh K. and Martin U., Large hydrovolcanic field in the Pannonian Basin: general characteristics of the Bakony-Balaton Highland Volcanic Field, Hungary, *Acta Vulcanol.* **11** (2), 1999a, 271–282.

Németh K. and Martin U., Late Miocene paleo-geomorphology of the Bakony-Balaton Highland Volcanic Field (Hungary) using physical volcanology data, *Z. Geol. Wiss.* **43** (4), 1999b, 417–438, N. F..

Németh K., Martin U. and Harangi S., Miocene phreatomagmatic volcanism at Tihany (Pannonian Basin, Hungary), *Journal of Volcanology and Geothermal ResearchJ. Volcanol. Geotherm. Res.* **111** (1–4), 2001, 111–135.

Oeser M., Ruprecht P. and Stefan W., Combined Fe-Mg chemical and isotopic zoning in olivine constraining magma mixing-to-eruption timescales for the continental arc volcano Irazú (Costa Rica) and Cr diffusion in olivine, *American MineralogistAm. Mineral.* **103** (4), 2018, 582–599.

Paton C., Hellstrom J., Paul B., Woodhead J. and Hergt J., Iolite: Freeware for the visualisation and processing of mass spectrometric data, *Journal of Analytical Atomic SpectrometryJ. Anal. At. Spectrom.* **26**, 2011, 2508–2518.

Paul B., Paton C., Norris A., Woodhead J., Hellstrom J., Hergt J. and Greig A., CellSpace: Aa module for creating spatially registered laser ablation images within the Iolite freeware environment, *Journal of Analytical Atomic SpectrometryJ. Anal. At. Spectrom.* **27**, 2012, 700–706.

Petrelli M., Perugini D., Alagna K.E., Poli G. and Peccerillo A., Spatially resolved and bulk trace element analysis by laser ablation - inductively coupled plasma - mass spectrometry (LA-ICP-MS), *Periodico di Mineralogia* **77**, 2008, 3–21.

Petrelli M., Morgavi D., Vetere F.P. and Perugini D., Elemental imaging and petro-volcanological Aapplications of an Iimproved laser ablation inductively Ccoupled quadrupole plasma mass spectrometry, *Periodico di Mineralogia* **85**, 2016, 25–39.

Petrus J.A., Chew D.M., Leybourne M.I. and Kamber B.S., A new approach to laser-ablation inductively-coupled-plasma mass-spectrometry (LA-ICP-MS) using the flexible map interrogation tool 'Monocle, *Chemical GeologyChem. Geol.* **463**, 2017, 76–93.

Re G., Palin J.M., White J.D.L. and Parolari M., Unravelling the magmatic system beneath a monogenetic volcanic complex (Jagged Rocks Ccomplex, Hopi Buttes, AZ, USA), *Contributions to Mineralogy and PetrologyContrib. Mineral. Petrol.* **172** (11), 2017, 94.

Reubi O. and Blundy J., A dearth of intermediate melts at subduction zone volcanoes and the petrogenesis of arc andesites, *Nature* **461**, 2009, 1269–1273.

Reubi O., Nicholls I.A. and Kamenetsky V.S., Early mixing and mingling in the evolution of basaltic magmas: evidence from phenocryst assemblages, Slamet Volcano, Java, Indonesia, *J. Volcanol. Geotherm. Res.* **119** (1–4), 2002, 255–274.

Roeder P.L., Chromite: from the fiery rain of chondrules to the Kilauea Iki lava lake, ~~*Can Mineral.*~~*Can. Mineral.* **32** (4), 1994, 729–746.

Roeder P.L., Thornber C., Poustovetov A. and Grant A., Morphology and composition of spinel in Pu'u 'O'o lava (1996–1998), Kilauea volcano, Hawaii, ~~*Journal of Volcanology and Geothermal Research*~~*J. Volcanol. Geotherm. Res.* **123** (3~~-~~–4), 2003, 245–265.

Ruprecht P. and Plank T., Feeding andesitic eruptions with a high-speed connection from the mantle, *Nature* **500**, 2013, 68.

Sato H., Nickel content of basaltic magmas: identification of primary magmas and a measure of the degree of olivine fractionation, *Lithos* **10** (2), 1977, 113–120.

Seghedi I., Downes H., Vaselli O., Szakács A., Balogh K. and Pécskay Z., Post-collisional Tertiary-Quaternary mafic alkalic magmatism in the Carpathian-Pannonian region: a review, *Tectonophysics* **393** (1~~-~~–4), 2004, 43–62.

Simkin T. and Smith J.V., Minor-Element ~~D~~distribution in Olivine, *J. Geol.* **78** (3), 1970, 304–325.

Smith D.R. and Leeman W.P., Chromian spinel-olivine phase chemistry and the origin of primitive basalts of the southern Washington Cascades, ~~*Journal of Volcanology and Geothermal Research*~~*J. Volcanol. Geotherm. Res.* **140** (1~~-~~–3), 2005, 49–66.

Smith I.E.M. and Németh K., Source to surface model of monogenetic volcanism: a critical review, In: Németh K., Carrasco-Nuñez G., Aranda-Gomez J.J. and Smith I.E.M., (Eds.), *Monogenetic Volcanism,* 2017, The Geological Society Publishing House; Bath, UK.

Smith I.E.M., Blake S., Wilson C.J.N. and Houghton B.F., Deep-seated fractionation during the rise of a small-volume basalt magma batch: Crater Hill, Auckland, New Zealand, *Contrib. Mineral. Petrol.* **155** (4), 2008, 511–527

Sobolev A.V., Hofmann A.W., Sobolev S.V. and Nikogosian I.K., An olivine-free mantle source of Hawaiian shield basalts, *Nature* **434**, 2005, 590.

Sobolev A.V., Hofmann A.W., Kuzmin D.V., Yaxley G.M., Arndt N.T., Chung S.-L., Danyushevsky L.V., Elliott T., Frey F.A., Garcia M.O., Gurenko A.A., Kamenetsky V.S., Kerr A.C., Krivolutskaya N.A., Matvienkov V.V., Nikogosian I.K., Rocholl A., Sigurdsson I.A., Sushchevskaya N.M. and Teklay M., The amount of recycled crust in ~~S~~sources of mantle-derived melts, *Science* **316** (5823), 2007, 412.

Sohn Y.K., Cronin S.J., Brenna M., Smith I.E.M., Németh K., White J.D.L., Murtagh R.M., Jeon Y.M. and Kwon C.W., Ilchulbong tuff cone, Jeju Island, Korea, revisited: ~~A~~a compound monogenetic volcano involving multiple magma pulses, shifting vents, and discrete eruptive phases, ~~*Geological Society of America Bulletin*~~*Geol. Soc. Am. Bull.* **124** (3~~-~~–4), 2012, 259–274.

Stormer J.C., Calcium zoning in olivine and its relationship to silica activity and pressure, ~~*Geochimica et Cosmochimica Acta*~~*Geochim. Cosmochim. Acta* **37** (8), 1973, 1815–1821.

Streck M.J., Mineral textures and zoning as ~~E~~evidence for open system processes, In: Putirka K.D. and Tepley F.J., III , (Eds.), *Minerals, Inclusions and Volcanic Processes,* 2008, Mineralogical Society of America & Geochemical Society, 595–622.

Strong M. and Wolff J., Compositional variations within scoria cones, *Geology* **31** (2), 2003, 143–146.

Szabó C., Falus G., Zajacz Z., Kovács I. and Bali E., Composition and evolution of lithosphere beneath the Carpathian-Pannonian Region: a review, *Tectonophysics* **393** (1~~-~~–4), 2004, 119–137.

Tari G., Dövényi P., Horváth F., Dunkl I., Lenkey L., Stefanescu M., Szafián P. and Tóth T., Lithospheric structure of the Pannonian Basin derived from seismic, gravity and geothermal data, In: Durand B., Jolivet L., Horváth F. an Séranne M., (Eds.), *The Mediterranean Basins: Tertiary ~~e~~Extension within the Alpine ~~o~~Orogen, Special Publication* 1999, Geological Society; London, 215–250.

Ubide T. and Kamber B.S., Volcanic crystals as time capsules of eruption history, ~~*Nature Communications*~~*Nat. Commun.* **9** (1), 2018, 326.

Ubide T., Galé C., Larrea P., Arranz E. and Lago M., Antecrysts and their effect on rock compositions: the cretaceous lamprophyre suite in the Catalonian Coastal Ranges (NE Spain), *Lithos* **206–207**, 2014, 214–233.

Ubide T., McKenna C.A., Chew D.M. and Kamber B.S., High-resolution LA-ICP-MS trace element mapping of igneous minerals: ~~i~~in search of magma histories, ~~*Chemical Geology*~~*Chem. Geol.* **409**, 2015, 157–168.

van Otterloo J., Raveggi M., Cas R.A.F. and Maas R., Polymagmatic ~~A~~activity at the monogenetic Mt Gambier volcanic ~~C~~complex in the newer volcanics province, SE Australia: new insights into the occurrence of intraplate volcanic ~~A~~activity in Australia, ~~*Journal of Petrology*~~*J. Petrol.* **55** (7), 2014, 1317–1351.

Wijbrans J., Németh K., Martin U. and Balogh K., 40Ar/39Ar geochronology of Neogene phreatomagmatic volcanism in the western Pannonian Basin, Hungary, ~~*Journal of Volcanology and Geothermal Research*~~*J. Volcanol. Geotherm.*

E-Extra

Single spot measurements were carried out on the cores, growth zones and rims of olivine crystals showing diverse textures, zoning patterns and compositions. Data were collected for Li, Na, Al, P, Ca, Sc, Ti, V, Cr, Mn, Co, Ni, Zn, Y, Zr and Nb, using spot sizes of 15 and 25 µm, depending on the size of the cores and on the width of the zones and rims being analyzed, with a repetition rate and fluence of 8 Hz and 3.5 J/cm^2, respectively. Dwell times were 10 ms per analyte. The NIST 610 reference material was used as the calibration standard, and USGS BCR2G glass was our quality control. Si concentrations determined by EMPA were used as an internal standard. Data Reduction was carried out using the "Trace_Elements" Data Reduction Scheme of the Iolite v.3 software package (Paton et al., 2011). Under the reported analytical conditions, precision and accuracy are typically better than 10% (Petrelli et al., 2008, 2016). Repeated analyses (n = 10) of the USGS BCR2G reference material performed in the same analytical session of the data reported in present study confirmed the expected figures of merits with the only slight deviations of Cr and P, showing divergences from the reference values of 11 and 13 %, respectively (Supplementary Table 5).

The juvenile pyroclasts contain a remarkably diverse mineral assemblage (≤ 4 mm-sized crystals) of olivine + clinopyroxene + orthopyroxene + spinel + amphibole + quartz + K-feldspar ± plagioclase. In addition, they also comprise various xenoliths (≤ 7 mm) of peridotite, sandstone, siltstone and mudstone (Fig. 2A–B). The minerals recognized in the juvenile pyroclasts show highly variable appearances with a significant amount of crystals showing disequilibrium textures (Supplementary Fig. 1): rounded and embayed olivines with diffuse rims; anhedral and ragged orthopyroxenes with fine-grained reaction rims; subhedral clinopyroxenes with variably resorbed, colorless (under the optical microscope) cores (often with spongy parts) and pale brown, sector zoned rims; anhedral and rounded spinels with spongy rims; ragged and anhedral amphiboles often with reaction rims. All these textural features suggest a xenocrystic origin for these minerals (olivines, orthopyroxenes, spinels, amphiboles and rounded clinopyroxene cores) which are originated from the subcontinental lithospheric mantle (together with the peridotite xenoliths). Very similar mineral assemblages characterized by the same disequilibrium textures were reported from the alkaline basalts of the adjacent Füzes-tó scoria cone and Bondoró-hegy eruptive centers (Fig. 1B), where these anhedral olivines, orthopyroxenes, spinels and colorless clinopyroxene cores were proved to be lithospheric mantle-derived xenocrysts based on their textures and compositions (Jankovics et al., 2009, 2013, 2016). The Fekete-hegy samples contain anhedral, resorbed quartz and K-feldspar crystals, which are interpreted as xenocrysts derived from the crust (together with the siliciclastic xenoliths). Glomerocrysts of olivine and/or clinopyroxene are often observed. The microphenocrysts (≤ 150 µm) in the juvenile components are olivine, clinopyroxene, plagioclase and Fe-Ti-oxides, and the groundmass consists of the same mineral phases with the addition of a small amount of glass.

Some differences can be observed in the phreatomagmatic products between the three sample locations (L1, L3 and L5) (Fig. 1C). For example, they differ in abundance and type of lithic fragments, the appearance and size of the sideromelane glass shards, and the amount of the xenocrysts in the juvenile pyroclasts. In addition, at sample location 1 (L1) the deposits contain abundant megacrysts (0.5–3 cm) of amphibole ≫ clinopyroxene ≫ mica, which are present as independent pyroclasts as well as inside the juvenile basalt fragments. Compared to L1 and L3, the juvenile basalt fragments from L5 comprise the largest amount of crustal siliciclastic xenoliths which show textural features resulting from partial melting by the host basaltic magma (Supplementary Fig. 1A).

Previous whole-rock geochemical data from the northern and southern effusive rocks, as well as one of the scoria cones (corresponding to our L6) of the Fekete-hegy volcanic complex were reported by Jugovics (1976) and Embey-Isztin et al. (1993). For this study, with the exception of L3 where the juvenile basalt fragments are more altered, samples were analyzed from each of the studied sample localities (Fig. 1C): juvenile basalt fragments from the lapillistones and lapilli tuffs (unit 1), lavas (unit 2), scoria and volcanic bombs (unit 3). New whole-rock compositions are given in Supplementary Table 1.

Aside from the striking differences observed between the appearance and modal mineralogy of the basaltic rocks from unit 1 and unit 2–3, there are also significant distinctions between the textures, zoning and chemistry of their olivine crystals. While the olivines in unit 1 show a remarkably large diversity, the olivines of unit 2 and unit 3 are simple and uniform. Olivine compositions measured from all the three eruptive units are plotted in Fig. 4A–B, and representative major and trace element compositions are given in Table 1. The complete olivine dataset is available in Supplementary Tables 2 and 3.

Trace element maps displaying intra-crystal compositional variations for each olivine type are presented in Fig. 8. The different zoning patterns shown in the BSE images (Figs. 5, 8) and described above for each olivine type (Fig. 7) are clearly reproduced in the high-resolution trace element crystal maps. The maps illustrate that the intra-crystal compositional changes of trace elements Ni, Cr, Mn and Zn mostly correlate with Fo contents. Ni and Fo variations correlate positively across olivine types I, II, III and V, but show negative correlation in the representative type IV crystal (Fig. 8D). Cr correlates positively with Fo across the type I, II, III and IV crystals, however this is not the case in the type V olivines. The representative type V crystal map (Fig. 8E) shows that both the core and the growth zone (which significantly differ in Fo; Figs. 6–7) have the same, low-Cr concentrations surrounded by a Cr-richer rim. The other mapped type V crystal (Fig. 5G, Supplementary Fig. 2), however, displays a growth zone that is poorer in Cr than the core (corresponding to the Fo variation) and it is followed by a Cr-richer rim. Mn and Zn behave similarly and show negative correlation with Fo in all olivine types excepting the type IV crystal where these two elements change oppositely (Mn correlates positively but Zn negatively with Fo).

The type III olivine cores together with sparse type V olivine cores define environment D. Although a similarly fractionated environment to E, environment D differs with regard to several elements in its olivines (Figs. 7, 10B, 11). It is important to note that aside from the smaller olivines, numerous large (1–4.5 mm) crystals occur as the cores of type III olivines (Fig. 5D). One of the studied samples contains several such large (3–5 mm) olivine crystals attached to a ~2 cm-sized clinopyroxene megacryst (colorless under the optical microscope) (Supplementary Fig. 3). These olivine grains show very similar appearances as the large type III olivine cores. They consist of numerous subgrains, mainly in their marginal parts. A number of clinopyroxene and amphibole megacrysts were found at L1, which have the same appearances and textural features as the well-studied clinopyroxene and amphibole megacrysts commonly found in other alkaline basaltic volcanics from the Bakony-Balaton Highland Volcanic Field (e.g., Embey-Isztin et al., 1990; Dobosi et al., 2003a; Jankovics et al., 2013, 2016). They generally occur together with pyroxenite (Type II) xenoliths consisting of clinopyroxene + olivine + spinel ± amphibole. Based on their major and trace element and isotopic characteristics, these megacrysts and pyroxenite xenoliths were inferred to share a common origin representing fragments of igneous cumulates crystallized from earlier alkaline basaltic magmas which did not reach the surface. These earlier magmas stalled and accumulated in the uppermost part of the lithospheric mantle, near the crust–mantle boundary and crystallized as veins, dykes and sills characterized by compositions very similar to those representing the host alkaline basalts (e.g., Embey-Isztin et al., 1990; Dobosi et al., 2003a; Jankovics et al., 2013, 2016). Considering the co-existence of the above-mentioned large olivine grains with a clinopyroxene megacryst in our studied sample, and the appearance of the large type III olivine cores (textural features implying disaggregation; Fig. 5D), we can interpret the type III olivine cores as originating from the same igneous cumulates as the clinopyroxene and amphibole megacrysts and the pyroxenite xenoliths. Assuming a clinopyroxene + amphibole + olivine mineral assemblage for these earlier accumulated alkaline basaltic magmas, this origin can be also supported by the composition of type III olivine cores. The intermediate Fo and Ni contents of the type III olivine cores can be attributed to olivine crystallization, their low Cr concentrations could be the result of co-crystallization of clinopyroxene and their lower Ca contents may have been caused by the co-crystallization of both clinopyroxene and amphibole. Additionally, it can be assumed that during slow cooling and crystallization, these olivine crystals equilibrated, resulting in their quite homogeneous compositions observed within individual type III olivine cores. This scenario also explains why their Fo and Ni concentrations are similar to those of the olivines crystallized from environment E (because the earlier stalled alkaline basaltic magmas, represented by the cumulates, are similar in composition to the final crystallization regime, i.e., environment E).

E-component

The following are the supplementary data related to this article.

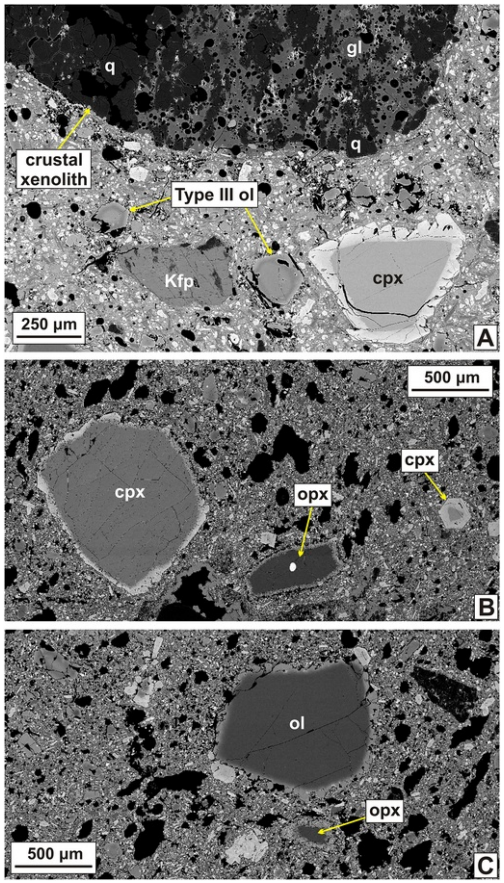

Supplementary Fig. 1 (A) Textural appearance of a rounded, partially melted crustal siliciclastic xenolith consisting of quartz (q) and vesiculated glass (gl) and (A-C) characteristics of variable xenocrysts in the juvenile basalt fragments of unit 1 samples (from L5). K-feldspar (Kfp) xenocrysts originate from the upper/middle crust probably together with the siliciclastic xenoliths, ~~whilst~~ while the olivine (ol), clinopyroxene (cpx) and orthopyroxene xenocrysts (opx) derive from the subcontinental lithospheric mantle. Clinopyroxene xenocrysts occur as anhedral, resorbed cores overgrown by phenocrystic clinopyroxene (A-B) and they often have a spongy margin (or more extended spongy parts) as well (B). Orthopyroxene xenocrysts are usually surrounded by a fine-grained reaction rim (consisting of olivine + Si-rich glass + clinopyroxene ± spinel) (B–C) and sometimes they contain poikilitically enclosed spinel (B).

alt-text: Supplementary Fig. 1

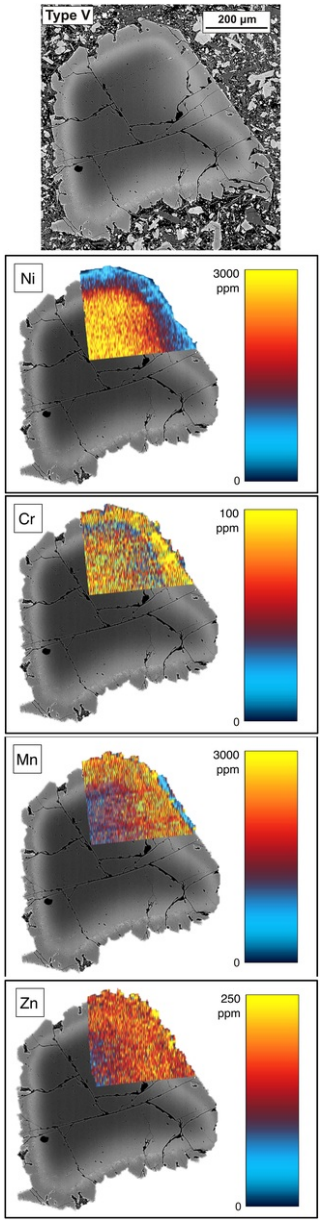

Supplementary Fig. 2 High-resolution trace element crystal maps (Ni, Cr, Mn and Zn) and corresponding BSE image of the type V olivine shown in Fig. 5G (unit 1).

alt-text: Supplementary Fig. 2

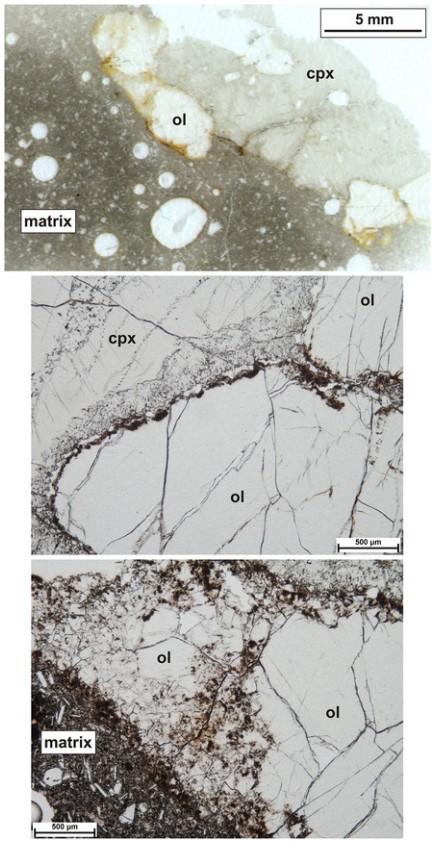

Supplementary Fig. 3 One of the studied thin sections from L1 (juvenile basalt fragment; unit 1) that contains several large (3–5 mm) olivine crystals attached to a ~2 cm-sized clinopyroxene megacryst (colorless under the optical microscope). These olivine grains consist of numerous subgrains, mainly in their marginal parts, and show very similar appearances as the large type III olivine cores (like in Fig. 5D).

alt-text: Supplementary Fig. 3

Multimedia Component 1

Supplementary Table 1 Whole-rock compositions of the studied samples from the three eruptive units.

alt-text: Supplementary Table 1

Multimedia Component 2

Supplementary Table 2 Major element compositions (wt.%) of the studied olivine crystals from the three eruptive units.

alt-text: Supplementary Table 2

Multimedia Component 3

Supplementary Table 3 Trace element concentrations (ppm) of the studied olivine crystals from unit 1.

alt-text: Supplementary Table 3

Multimedia Component 4

Supplementary Table 4 Compositions of the studied olivine-hosted spinel inclusions from the three eruptive units.

alt-text: Supplementary Table 4

Multimedia Component 5

Supplementary Table 5 Repeated analyses (n=10) of the USGS BCR2G reference material, utilized as quality control. The table reports the average values of the analyzed elements, the resulting standard deviations (1 s), and the reference values by Gao et al., 2002 (Li, Sc, Ti, V, Cr, Mn, Co, Ni, Zn, Y, Zr, and Nb; LA-ICP-MS) and Jochum et al., 2005 (Na, Al, P, and Ca; EPMA).

alt-text: Supplementary Table 5

Highlights

- A compound monogenetic basaltic system with distinct eruption episodes.
- High-resolution analysis of diversely zoned olivines and their spinel inclusions.
- Complex magmatic system with various magmatic environments and petrogenetic processes.
- Significant change during the evolution of the sub-volcanic magmatic system.

Queries and Answers

Query:

Citation "Harangi, 2001" has not been found in the reference list. Please supply full details for this reference.

Answer: Harangi, S., 2001. Volcanology and petrology of the Late Miocene to Pliocene alkali basaltic volcanism in the Western Pannonian Basin. In: Ádám, A., Szarka, L. (Eds.), PANCARDI 2001 Field Guide, Sopron, pp. 51–81.

Query:

Please check the presentation of data and layout of Tables 1 and 2 if correct.

Answer: I added an instruction both to Table 1 and Table 2, additionally I made some corrections in Table 2.

Query:

Your article is registered as a regular item and is being processed for inclusion in a regular issue of the journal. If this is NOT correct and your article belongs to a Special Issue/Collection please contact m.ayyamperumal@elsevier.com immediately prior to returning your corrections.

Answer: Yes

Query:

Please confirm that given names and surnames have been identified correctly and are presented in the desired order, and please carefully verify the spelling of all authors' names.

Answer: The surname of the first author is only "Jankovics" ("M." and "Éva" are both given names).

Query:

The author names have been tagged as given names and surnames (surnames are highlighted in teal color). Please confirm if they have been identified correctly.

Answer: The surname of the first author is only "Jankovics" ("M." and "Éva" are both given names).

Query:

Please confirm that the provided email m.eva.jankovics@gmail.com is the correct address for official communication, else provide an alternate e-mail address to replace the existing one, because private e-mail addresses should not be used in articles as the address for communication.

Answer: This email address is correct for official communication.

Query:

Please check whether the designated corresponding author is correct, and amend if necessary.

Answer: The surname of the corresponding author is only "Jankovics" ("M." and "Éva" are both given names).

Query:

Uncited references: This section comprises references that occur in the reference list but not in the body of the text. Please position each reference in the text or, alternatively, delete it. Thank you.

Answer: I deleted these uncited references.

Query:

Have we correctly interpreted the following funding source(s) and country names you cited in your article: "European Union and the State of Hungary; European Social Fund, European-Union; Erasmus+, European-Union".

Answer: Yes

Query:

Hirano et al. (2004) was a duplicate and was thus removed from the Reference list. Please check if appropriate.

Answer: Yes.